

Title comes here

Yossi Michaeli

March 28, 2010

Acknowledgment

Contents

1	Introduction	9
2	Electronic Properties of Semiconductors	10
2.1	Crystal Schrödinger Equation	11
2.1.1	Introduction	11
2.1.2	Bloch's Theorem	13
2.1.3	The $\mathbf{k} \cdot \mathbf{p}$ Method	15
2.1.3.1	Introduction	15
2.1.3.2	Symmetry Properties of Wavefunctions	16
2.1.3.3	Löwdin-Renormalization	21
2.2	The $\mathbf{k} \cdot \mathbf{p}$ Envelope Function Method	23
2.2.1	Introduction	23
2.2.2	$\mathbf{k} \cdot \mathbf{p}$ Envelope Function Ansatz	24
2.2.3	The Zinc-blende Models	26
2.2.3.1	Direct Interaction	26
2.2.3.2	Remote Contributions	28
2.2.3.3	Spin-Orbit Interaction	30
2.2.4	Two Band Model	37
3	Free Carriers Optical Transitions	45
3.1	Second Quantization	46
3.1.1	Introduction	46
3.1.1.1	Single Particle Hamiltonian	48
3.1.1.2	Two Particle Hamiltonian: Coulomb Interac- tion	49

3.1.1.3	Particle – Electromagnetic Field Interaction Hamiltonian	49
3.1.2	Bloch States Formulation	51
3.1.2.1	Normalization	52
3.1.2.2	Lattice-Cell Average	52
3.1.2.3	The Kinetic Term	53
3.1.2.4	The Interaction Term	54
3.1.3	Holes	55
3.1.4	Carrier Statistics	56
3.2	Transitions Calculation	57
3.2.1	Introduction	57
3.2.2	Quantum Microscopic Polarization	59
3.2.3	Heisenberg's Equation of Motion	60
3.2.4	Solving the Free Carrier Equation	62
3.3	Spontaneous Emission	63
3.4	Dipole Matrix Element	65
4	Coulomb Correlated Optical Transitions	68
4.1	Second Quantization	69
4.1.1	Introduction	69
4.1.2	Diagonal Approximation	71
4.1.3	Holes	72
4.2	Transitions Calculation	73
4.2.1	Equations of Motion	73
5	Semiconductor Microcavity	75
5.1	Optical Resonator	75
5.2	Distributed Bragg Reflector	77
5.2.1	Transfer Matrix Method (TMM)	79
5.3	Microvity Optical Characteristics	84
5.3.1	Microcavity Reflection Spectrum	84
5.3.2	Microcavity Confined Photon	87
	Bibliography	88

List of Figures

2.1	Schematic representation of electronic functions in a crystal (a) potential plotted along a row of atoms, (b) free electron wave function, (c) amplitude factor of Bloch function having the periodicity of the lattice, and (d) Bloch function ψ (after (author?) [37])	14
2.2	Schematic band structure classification in the Löwdin pertur- bation theory.	22
2.3	Band structure of bulk <i>GaAs</i> around the Γ point at room temperature, calculated using the $8 \times 8 \mathbf{k} \cdot \mathbf{p}$ for two crystal directions.	33
2.4	Contours of constant energy within any [100] plane of k -space for the heavy (right) and light (left) hole subbands in bulk <i>GaAs</i> . The energy spacing between each contour level is $0.5 meV$ for the HH band and $3 meV$ for the LH band. The effective HH mass is much larger along the [110] direction than along the [100] direction, as indicated by the larger contour spacing. The effective LH mass is seen to be much more isotropic (after (author?) [44]).	40
2.5	The "in-plane" subband structure of the quantum well in the conduction band. Within the plane of the well, the electron still behaves like a "free" electron. Thus, for each quantized level, a parabolic energy subband exist (after (author?) [44]).	41

2.6	At any one energy on a bulk material, we can find four wavevectors corresponding to the heavy and light hole bands. An eigenstate of the Hamiltonian in a quantum well is then made of a linear combination of the bulk plane waves corresponding to those wave vectors. The amplitudes A_{\pm} and B_{\pm} in (a) correspond, respectively, to $\pm k_{z1}$ (light hole) and $\pm k_{z2}$ in (b) for the well layer of the quantum well (<i>GaAs</i> throughout this thesis). In the barriers (<i>AlGaAs</i>) a similar mechanism is employed. The boundary conditions at the interfaces then determine the energy eigenvalues and the coefficients.	42
2.7	(a) Valence subbands dispersion relations calculated for a 100 wide <i>GaAs</i> / <i>Al_{0.3}Ga_{0.7}As</i> quantum well, for [100] crystal plane. The subbands are named after their dominant character at the zone center ($k_t = 0$). (b) The ratio between the density of states of the valence subbands and the first conduction subband, calculated for the same structure.	44
5.1	Fabry-Perot etalon multiple reflections.	76
5.2	Resonator transmittance function for various values of mirror reflectance R . $\delta\lambda$ is the full-width half-maximum of the transmission band.	77
5.3	Schematic illustration of a Distributed Bragg Reflector (DBR). z represents the growth direction of the layered structure. . . .	78
5.4	Simulation of a DBR structure with 35 alternating high and low layers, where (a) is the refractive index profile as a function of the growth axis, (b) the amplitude and phase of the normal incidence reflection function this structure as a function of normalized wavelength, λ/λ_c , and (c) the same amplitude as a function of the phase acquired by the EM field at each layer, $\phi = \frac{2\pi l_i n_i}{\lambda}$	83
5.5	Microcavity schematic structure.	85

- 5.6 Simulation of a microcavity with two DBR's with 35 alternating high and low refractive index layers each, where (a) is the refractive index profile as a function of the growth axis, (b) the amplitude and phase of the normal incidence reflection function this structure as a function of normalized wavelength, λ/λ_c , and (c) the same amplitude as a function of the phase acquired by the EM field at each layer, $\phi = \frac{2\pi l_i n_i}{\lambda}$. The inset in (c) shows the reflection profile in the vicinity of $\phi = \frac{\pi}{2}$ 86

List of Tables

2.1	Symmetry operations of the group T_d using the Schönflies notation (notations after (author?) [43]).	18
2.2	Basis functions of the tetrahedral symmetry group T_d	19
2.3	Direct products of the Γ_{15} representation with all representations of T_d (after (author?) [43]).	20
2.4	The non-vanishing momentum matrix elements between the states corresponding to different irreducible representations of the tetrahedral symmetry group. A zero denotes a vanishing and X a non-vanishing element.	20

Abstract

Chapter 1

Introduction

Chapter 2

Electronic Properties of Semiconductors

The optical properties of nanostructures are intimately connected to the electronic states, the response of electrons within the atomic lattice to external perturbations. As such, a precise knowledge of the electronic properties is required for a proper device analysis. In bulk semiconductors, the lattice periodicity and its symmetry leads to the formation of electronic bands, continuously (within the band) relating the crystal momentum \mathbf{k} of an electron to its energy $E_n(\mathbf{k})$. The combination of different materials within a nanostructure breaks the symmetry of the semiconductor crystal, leading to *quantization effects*, i.e. modifications of the electronic properties from their bulk properties. These modifications have a pronounced impact on the electronic and optical properties of nanostructures. The present chapter covers the theory of the calculation of the electronic states in nanostructures using the *envelope function method* (EFM).

The first section contains an extensive introduction to the Schrödinger equation within a semiconductor crystal, which will later also serve as the basis for the analysis of optical effects covered in Chapter [chapter number for the optical effects](#) and the many body effects in optical spectra in Chapter [chapter number for the many body effects](#) .

After introducing certain approximations to the crystal Schrödinger equa-

tion, the concept of solving the resulting single-particle Schrödinger equation using the bulk $\mathbf{k}\cdot\mathbf{p}$ method is presented. The subsequent section derives the equations of the $\mathbf{k}\cdot\mathbf{p}$ envelope function method used in nanostructures and simultaneously introduces the $\mathbf{k}\cdot\mathbf{p}$ model for zinc-blende crystals. Note that the presented discussion doesn't include the influence of strain effects on the electronic properties.

2.1 Crystal Schrödinger Equation

2.1.1 Introduction

The total Hamiltonian of all electrons, atoms and the electro-magnetic field of a solid state crystal is given by

$$H = \sum_i \frac{1}{2m_i} (\mathbf{p}_i - ez_i\mathbf{A}(\mathbf{r}_i))^2 + \frac{\epsilon_0}{2} \int (\mathbf{E}^2 + c_0^2\mathbf{B}^2) d\mathbf{r} \quad (2.1)$$

In the second term \mathbf{E} denotes the electric- and \mathbf{B} the magnetic field. These fields are related to the vector potential \mathbf{A} and the scalar potential ϕ via ?]

$$\mathbf{E} = -\frac{\partial\mathbf{A}}{\partial t} - \nabla\phi \quad (2.2)$$

$$\mathbf{B} = \nabla \times \mathbf{A}. \quad (2.3)$$

In the first term of 2.1, e is the elementary charge, z_i is the charge of particle i in units of e (-1 for electrons) and m_i denotes the particle mass. The term $\mathbf{p}_i - ez_i\mathbf{A}(\mathbf{r}_i)$ is the mechanical momentum of particle i , which is invariant to our gauge choice (see below) for \mathbf{A} and ϕ . The electrical field term \mathbf{E}^2 holds both transverse and longitudinal contributions. In the following discussion we assume a Coulomb gauge for the vector potential, i.e. $\nabla \cdot \mathbf{A} = 0$?]. In this gauge the term $\frac{\partial\mathbf{A}}{\partial t}\nabla\phi$ in \mathbf{E}^2 vanishes, and so we can split this term to the transverse and longitudinal contributions $\mathbf{E}^2 = \mathbf{E}_t^2 + \mathbf{E}_l^2$. Using Poisson's equation, the longitudinal contribution can be written in terms of the charge

density

$$\int \mathbf{E}_l^2 d\mathbf{r} = \int (\nabla \phi)^2 d\mathbf{r} = \langle \phi \nabla \phi \rangle - \int \phi \nabla^2 \phi d\mathbf{r} = \int \phi \frac{\rho}{\epsilon_0} d\mathbf{r}. \quad (2.4)$$

Next, the contributions to ϕ are distinguished between internal ϕ_{int} and external ϕ_{ext} , where the internal contributions are created by the crystal electrons and atomic cores. The internal contributions are given by the longitudinal Coulomb interaction between the charged particles i and j

$$V_{i,j} = \frac{e^2 z_i z_j}{4\pi\epsilon_0 |\mathbf{r}_i - \mathbf{r}_j|}, \quad (2.5)$$

with unit charges z_i and z_j . The external contribution are

$$V_{ext} = \sum_i z_i e \phi_{ext}(\mathbf{r}_i). \quad (2.6)$$

The crystal Hamiltonian for electrons i, j and atoms I, J then reads

$$\begin{aligned} H = & \underbrace{\sum_i \frac{(\mathbf{p}_i + e\mathbf{A})^2}{2m_0}}_{T_e} + \underbrace{\sum_I \frac{(\mathbf{p}_I + e z_I \mathbf{A})^2}{2m_I}}_{T_a} + \underbrace{\frac{1}{2} \sum_{i,j} \frac{e^2}{4\pi\epsilon_0 |\mathbf{r}_i - \mathbf{r}_j|}}_{V_{ee}} \\ & + \underbrace{\frac{1}{2} \sum_{I,J} \frac{e^2 z_I z_J}{4\pi\epsilon_0 |\mathbf{r}_I - \mathbf{r}_J|}}_{V_{aa}} - \underbrace{\frac{1}{2} \sum_{i,J} \frac{e^2 z_J}{4\pi\epsilon_0 |\mathbf{r}_i - \mathbf{r}_J|}}_{V_{ea}} + V_{ext} \\ & + \underbrace{\frac{\epsilon_0}{2} \int (\mathbf{E}_t^2 + c_0 \mathbf{B}^2) d\mathbf{r}}_{H_{EM}}, \end{aligned} \quad (2.7)$$

where T is the kinetic energy part of the Hamiltonian, and V the potential energy one. As the atoms have a much higher mass than the electrons, the Born-Oppenheimer approximation (**author?**) [43] can be used to separate the motion of electrons and atoms. The electrons will react on movements of the atoms instantaneously. Therefore, the interaction between ion cores and between electrons and ion cores can be concentrated into a potential $U(\mathbf{x})$,

leading to the final crystal electron Hamiltonian

$$H = \sum_i \left(\frac{(\mathbf{p}_i + e\mathbf{A}(\mathbf{r}_i))^2}{2m_0} + U(\mathbf{r}_i) \right) + \frac{1}{2} \sum_{i,j} \frac{e^2}{4\pi\epsilon_0|\mathbf{r}_i - \mathbf{r}_j|} + V_{ext} + H_{EM}. \quad (2.8)$$

The next step is to perform the *single electron approximation* or *mean field approximation* by assuming that the electron-electron interaction V_{ee} with the core- and valence electrons can also be concentrated into the potential $U(\mathbf{r})$. This step is necessary as solving the equation for 10^{23} explicitly considered electrons is an impossible task. The equation reduces to a single electron equation, where an electron experiences the mean-field potential $U(\mathbf{r})$. Within this step, the vector potential \mathbf{A} is restricted to external excitations, where the local oscillations within the crystal lattice are averaged out. Overall, the effect of the external electro-magnetic field on the atoms has been excluded. This approximation is usually justified in the case of weak fields and heavy atomic masses. The interaction between electrons and atoms is restricted to a frozen lattice. The interaction between the movement of the atoms and the electrons can be reintroduced using *phonons* (author?) [43], but this will be omitted throughout the thesis.

2.1.2 Bloch's Theorem

Assuming no external field, the time independent single electron Schrödinger equation to solve is given by

$$\left(-\frac{\hbar^2}{2m_0} \nabla^2 + U(\mathbf{r}) \right) \psi = E\psi. \quad (2.9)$$

For the moment, the crystal is assumed to be homogeneous and perfect. The potential $U(\mathbf{r})$ is periodic within the lattice (see Figure 2.1). For any translation vector \mathbf{R} mapping the infinite crystal lattice to itself, the potential

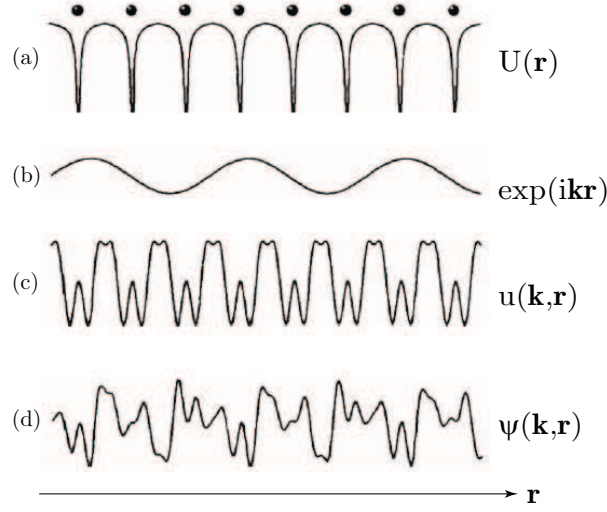


Figure 2.1: Schematic representation of electronic functions in a crystal (a) potential plotted along a row of atoms, (b) free electron wave function, (c) amplitude factor of Bloch function having the periodicity of the lattice, and (d) Bloch function ψ (after **author?**) [37]

obeys

$$U(\mathbf{r}) = U(\mathbf{r} + \mathbf{R}) \quad (2.10)$$

and the wavefunction $\psi_{n\mathbf{k}}$ can be expressed in the form known as *Bloch function*

$$\psi_{n\mathbf{k}} = u_{n\mathbf{k}}(\mathbf{r})e^{i\mathbf{k}\cdot\mathbf{r}}, \quad (2.11)$$

where $u_{n\mathbf{k}}(\mathbf{r})$ denotes the lattice periodic path with

$$u_{n\mathbf{k}}(\mathbf{r}) = u_{n\mathbf{k}}(\mathbf{r} + \mathbf{R}) \quad (2.12)$$

and the plane wave is the slowly modulating envelope. The $n\mathbf{k}$ are the quantum numbers indexing the solutions. Applying the differential operators to the plane wave and multiplying the equation on both sides from the left with $e^{-i\mathbf{k}\cdot\mathbf{r}}$ gives the equation for the lattice periodic functions as

$$\begin{aligned} H_{\mathbf{k},\mathbf{p}}(\mathbf{k})u_{n\mathbf{k}}(\mathbf{r}) &= \left(-\frac{\hbar^2}{2m_0}\nabla^2 + \frac{\hbar}{m_0}\mathbf{k}\cdot\mathbf{p} + \frac{\hbar^2k^2}{2m_0} + U(\mathbf{r}) \right) u_{n\mathbf{k}}(\mathbf{r}) \\ &= E_n(\mathbf{k})u_{n\mathbf{k}}(\mathbf{r}). \end{aligned} \quad (2.13)$$

An important consequence of the Bloch theorem is the fact that wavefunctions with different \mathbf{k} values are not coupled together (due to the slowly varying plane wave) and therefore 2.13 has a parametric dependence on the crystal momentum \mathbf{k} .

2.1.3 The $\mathbf{k} \cdot \mathbf{p}$ Method

2.1.3.1 Introduction

There is a vast number of methods to obtain solutions to Eq. 2.13. One of the most frequently used is the semi-empirical $\mathbf{k} \cdot \mathbf{p}$ method that serves to derive analytical expressions for the band structure, using symmetry arguments and experimental observations. The method was initially introduced by Bardeen and Seitz (see references in (author?) [15]) and applied by many researchers. It is particularly useful to describe the band structure for direct semiconductors used in optoelectronic devices at the Γ point of the Brillouin zone with a high precision.

Hereafter a short introduction of the general concepts will be given. These concepts will later reappear within the Envelope Function Methods (EFM). This introduction is mainly based on (author?) [43].

The basic idea within the $\mathbf{k} \cdot \mathbf{p}$ theory (author?) [28] is to solve 2.13 for an extremal point with high symmetry of the band structure, usually the Γ point at $\mathbf{k} = 0$. There, 2.13 reduces to

$$\left(-\frac{\hbar^2}{2m_0} \nabla^2 + U(\mathbf{r}) \right) u_{n0}(\mathbf{r}) = E_n(0) u_{n0}(\mathbf{r}). \quad (2.14)$$

The solutions $u_{n0}(\mathbf{r})$ are denoted as *zone-center* functions and span the complete Hilbert space of all solutions to 2.13. Therefore, one may express the lattice periodic functions $u_{n\mathbf{k}}(\mathbf{r})$ away from the Γ point in terms of the zone-center functions

$$u_{n\mathbf{k}}(\mathbf{r}) = \sum_{n'} a_{n\mathbf{k},n'} u_{n'0}(\mathbf{r}). \quad (2.15)$$

To obtain the coefficients $a_{n\mathbf{k},n'}$, the expansion 2.15 is inserted into 2.13, multiplied from the left by $u_{n0}(\mathbf{r})$ and integrated over the crystal unit-cell to

obtain

$$\sum_{n'} \left(\left(E_{n'}(0) + \frac{\hbar^2 k^2}{2m_0} \right) \delta_{nn'} + \frac{\hbar}{m_0} \mathbf{k} \cdot \mathbf{p}_{nn'} \right) a_{m\mathbf{k},n'} = E_m(\mathbf{k}) a_{m\mathbf{k},n'}, \quad (2.16)$$

where

$$\mathbf{p}_{nn'} = \int u_{n0}^*(\mathbf{r}) \mathbf{p} u_{n'0}(\mathbf{r}) d\mathbf{r} \quad (2.17)$$

is used to express the momentum matrix element between two zone-center Bloch functions. The above equation can obviously be written in matrix form, where a matrix entry is given by

$$h_{ij} = \left(E_j(0) + \frac{\hbar^2 k^2}{2m_0} \right) \delta_{ij} + \frac{\hbar}{m_0} \mathbf{k} \cdot \mathbf{p}_{ij} \quad (2.18)$$

and a diagonalization of the \mathbf{k} dependent, infinite matrix would lead to the exact coefficients and energies $E_m(\mathbf{k})$. As the matrix is continuous in \mathbf{k} , it is clear that the dispersion $E_m(\mathbf{k})$ will also be continuous.

As a remark, we can point out that 2.14 is not solved explicitly and no closed expression for $u_{n0}(\mathbf{r})$ is needed. Instead, the matrix 2.18 is constructed by using group theory to derive symmetry properties of the zone-center functions $u_{n0}(\mathbf{r})$. Using these symmetry properties, similarities and equivalences for the momentum matrix elements \mathbf{p}_{ij} can be deduced. A profound introduction into the group theory for semiconductors is beyond the current scope. A rough guideline illustrating the essence required by the $\mathbf{k} \cdot \mathbf{p}$ theory is presented here. An extensive presentation can be found in (author?) [43] and (author?) [6].

2.1.3.2 Symmetry Properties of Wavefunctions

Let $H(\mathbf{r}) = T + U(\mathbf{r})$ be the Hamiltonian in 2.14 with the kinetic operator T and crystal potential $U(\mathbf{r})$, and let G be the point group¹ of the crystal such

¹A *crystallographic point group* is a set of symmetry operations, like rotations or reflections, that leave a point fixed while moving each atom of the crystal to the position of an atom of the same kind. That is, an infinite crystal would look exactly the same before and after any of the operations in its point group. In the classification of crystals, each point group corresponds to a crystal class.

2. CHARACTER PROPERTIES OF SEMICONDUCTORS

that the symmetry operator $g \in G$, the crystal potential is invariant, i.e.

$$\forall g \in G, \quad U(g^{-1}\mathbf{r}) = U(\mathbf{r}).$$

The kinetic operator T is naturally invariant under the action of the elements in the point group G . Assuming that $\psi(\mathbf{r})$ is an eigenfunction of H with $H(\mathbf{r})\psi(\mathbf{r}) = E\psi(\mathbf{r})$ and applying the symmetry operator g , leads to

$$H(g^{-1}\mathbf{r})\psi(g^{-1}\mathbf{r}) = H(\mathbf{r})\psi(g^{-1}\mathbf{r}) = E\psi(g^{-1}\mathbf{r}).$$

Obviously $\psi'(\mathbf{r}) = \psi(g^{-1}\mathbf{r})$ is also an eigenfunction of the Hamiltonian operator $H(\mathbf{r})$ with eigenvalue E . The wavefunction $\psi'(\mathbf{r})$ might be the same wavefunction as $\psi(\mathbf{r})$ or might be linearly independent. Applying all symmetry operations $g \in G$ therefore results in a set of wavefunctions with the same eigenvalue E , spanning a function space

$$I_\psi = \{ \psi'(\mathbf{r}) | \psi'(\mathbf{r}) = \psi(g^{-1}\mathbf{r}) \quad \forall g \in G \}.$$

Now, the point group G is a closed group, meaning that for $g, f \in G : gf \in G$. Therefore, the function space I_ψ is invariant under the action of G ,

$$\psi(\mathbf{r}) \in I_\psi \Rightarrow \psi(g^{-1}\mathbf{r}) \in I_\psi.$$

Suppose that $\{\psi_0, \psi_1, \dots, \psi_N\}$ is the basis of the subspace I_ψ , which is assumed to be of the dimension N . The basis is denoted as being the *irreducible representation* of the group G . The desirable property deduced from group theory is that for every symmetry group, there are only a few distinct irreducible representations. Every irreducible representation describes an unique way how wavefunctions are transformed under the action of the elements of a symmetry group G . Therefore, the eigenfunctions of the crystal Hamiltonian H can be classified according to the irreducible representation they form. It is clear that each eigenfunction does only belong to one irreducible representation and it is clear that eigenfunctions corresponding to different irreducible representations are always orthogonal. In the following,

Type	Operation $(xyz) \rightarrow (\dots)$
E	(xyz)
$3C_2$	$(\bar{x}\bar{y}z), (xy\bar{z}), (\bar{x}y\bar{z})$
$8C_3$	$(zxy), (yzx), (\bar{y}z\bar{x}), (\bar{z}\bar{x}y), (\bar{y}\bar{z}x), (z\bar{x}\bar{y}), (y\bar{z}\bar{x}), (\bar{z}x\bar{y})$
$6C_4$	$(\bar{x}z\bar{y}), (\bar{x}\bar{z}y), (z\bar{y}\bar{x}), (\bar{z}\bar{y}x), (\bar{y}x\bar{z}), (y\bar{x}\bar{z})$
6σ	$(\bar{y}x\bar{z}), (yxz), (\bar{z}y\bar{x}), (zyx), (xzy), (x\bar{z}\bar{y})$

Table 2.1: Symmetry operations of the group T_d using the Schönflies notation (notations after (author?) [43]).

the theory will be focused on the zinc-blende crystal, for which the symmetry group of the Hamiltonian is T_d , the tetrahedral group. The elements are given by the 24 symmetry operations mapping a tetrahedron to itself. For an appropriate alignment and orientation, the symmetry operations are listed in Table 2.1. T_d has in total five distinct irreducible representations, which are commonly labeled as Γ_1 , Γ_2 , Γ_{12} , Γ_{15} and Γ_{25} . Γ_1 and Γ_2 are one dimensional representations, Γ_{12} is a two dimensional and Γ_{15} and Γ_{25} are three dimensional. The basis functions for all irreducible representations are given in Table 2.2. The representation Γ_1 is the identity representation, also denoted as trivial representation, leaving the wavefunction invariant. An atomic wavefunction with s -like symmetry transforms accordingly, i.e. is left unchanged under the action of the elements of the group T_d . An example of the Γ_1 representation is given by the conduction band at the Γ point of zinc-blende, direct bandgap III-V semiconductors. The conduction band at the Γ point is non-degenerate with a wavefunction obeying s -type symmetry. Another important irreducible representation is given by the top of the valence band at the Γ point. Neglecting the later considered spin-orbit splitting, the valence band is threefold degenerate, with p -type basis functions x, y and z , transforming under the action of T_d according to the elements of a vector. The p -type basis functions correspond to the representation Γ_{15} . The goal is now to use the introduced group theory to analyze the properties of the momentum matrix elements 2.17. The momentum operator \mathbf{p} is given by a

Γ_i	Dimension	Basis functions
Γ_1	1	xyz
Γ_2	1	$x^4(y^2 - z^2) + y^4(z^2 - x^2) + z^2(x^2 - y^2)$
Γ_{12}	2	$(x^2 - y^2), z^2 - \frac{1}{2}(x^2 + y^2)$
Γ_{15}	3	x, y, z
Γ_{25}	3	$x(y^2 - z^2), y(z^2 - x^2), z(x^2 - y^2)$

Table 2.2: Basis functions of the tetrahedral symmetry group T_d .

vector of three operators

$$\mathbf{p} = \begin{pmatrix} p_x \\ p_y \\ p_z \end{pmatrix},$$

obviously transforming like the elements of a vector. Therefore, the momentum operator forms an irreducible representation of Γ_{15} . The action of the momentum operator on wavefunctions of the irreducible representation Γ_j leads to a new expression. The corresponding representation is given by the *direct product* $\Gamma_{15} \otimes \Gamma_j$ (see **(author?)** [43], p. 46), as one has p_u acting on the basis function ψ_v for $u = x, y, z$ and $v = 1, \dots, N$. The direct product is not *irreducible*, but can be decomposed into a *direct sum* of irreducible representations

$$\Gamma_{15} \otimes \Gamma_j = \sum_u \oplus \Gamma_i. \quad (2.19)$$

Recall that functions not belonging to the same irreducible representation are orthogonal. Therefore, the matrix element $\langle \psi^{\Gamma_i} | \mathbf{p} | \psi^{\Gamma_j} \rangle$ between two wavefunctions belonging to the irreducible representation Γ_i and Γ_j is nonzero only if the direct sum 2.19 of the direct product $\Gamma_{15} \otimes \Gamma_j$ contains Γ_i . For the tetrahedral symmetry, the decomposition of the direct product into the direct sum is given in Table 2.3, from which the vanishing momentum matrix elements 2.17 can be calculated. They are given by the matrix in 2.4. Within the matrix, X denotes a non-vanishing and the 0 denotes a vanishing matrix element. In order to further reduce the number of unknowns, equivalent

2. CHARGE TRANSPORT PROPERTIES OF SEMICONDUCTORS

Direct product	Direct sum
$\Gamma_{15} \otimes \Gamma_1$	Γ_{15}
$\Gamma_{15} \otimes \Gamma_2$	Γ_{25}
$\Gamma_{15} \otimes \Gamma_{12}$	$\Gamma_{15} \oplus \Gamma_{25}$
$\Gamma_{15} \otimes \Gamma_{15}$	$\Gamma_{15} \oplus \Gamma_{25} \oplus \Gamma_{12} \oplus \Gamma_1$
$\Gamma_{15} \otimes \Gamma_{25}$	$\Gamma_{15} \oplus \Gamma_{25} \oplus \Gamma_{12} \oplus \Gamma_2$

Table 2.3: Direct products of the Γ_{15} representation with all representations of T_d (after (author?) [43]).

\mathbf{p}	$ \psi^{\Gamma_1}\rangle$	$ \psi^{\Gamma_2}\rangle$	$ \psi^{\Gamma_{12}}\rangle$	$ \psi^{\Gamma_{15}}\rangle$	$ \psi^{\Gamma_{25}}\rangle$
$\langle\psi^{\Gamma_1} $	0	0	0	X	0
$\langle\psi^{\Gamma_2} $	0	0	0	0	X
$\langle\psi^{\Gamma_{12}} $	0	0	0	X	X
$\langle\psi^{\Gamma_{15}} $	X	0	X	X	X
$\langle\psi^{\Gamma_{25}} $	0	X	X	X	X

Table 2.4: The non-vanishing momentum matrix elements between the states corresponding to different irreducible representations of the tetrahedral symmetry group. A zero denotes a vanishing and X a non-vanishing element.

matrix elements can be determined using the basis functions defined in Table 2.2 and symmetry operations of G . As an example, for the Γ_1 type conduction band, the only non-vanishing momentum matrix elements involve - according to Table 2.4 - only bands belonging to Γ_{15} . Γ_1 is represented by the function xyz and Γ_{15} by x, y and z . The only non-vanishing matrix element is of the type $\langle xyz | p_x | x \rangle$. For the other, e.g. $\langle xyz | p_x | z \rangle$, a rotation of the crystal by 180° around the rotation axis $[001]$ results in

$$\langle xyz | p_x | x \rangle = -\langle xyz | p_x | z \rangle,$$

which can only be met if the matrix element is zero.

2.1.3.3 Löwdin-Renormalization

While the matrix h_{ij} 2.18 is infinite, leading to an infinite number of bands, the assessment of light emission in optoelectronic devices usually requires only the knowledge of the lowest conduction and highest valence bands. For the relevant III-V semiconductors, the conduction and the valence bands lie at the Γ point energetically close together. Other bands can be regarded as being remote, so the interaction in-between these bands can be considered to dominate for the band structure of interest. In the model developed by Kane (**author?**) [29], therefore a submatrix h_{ij} of the conduction- and valence band at the Γ point is extracted out of 2.18 and diagonalized. Although the primary interest of Kane's model was to include spinorbit interaction, the missing interaction with remote bands resulted in a heavy-hole band structure, given by the free-electron dispersion, bending for a hole into the wrong direction. Luttinger and Kohn (**author?**) [34] included the interaction of remote states onto the selected set of bands, using Löwdin's perturbation theory (**author?**) [32]. The idea of Löwdin perturbation theory is to divide the bands in two classes S and R (see Fig. 2.2). Bands in class S are considered explicitly, i.e. the respective rows and columns of the matrix h_{ij} are kept. The bands R are considered being remote and their effect on the bands in class S are included in the submatrix of h_{ij} using perturbation theory. Hereby, the renormalized matrix elements are given by

$$h'_{ij} = h_{ij} + \sum_{\nu}^R \frac{h_{i\nu}h_{\nu j}}{E_i - h_{\nu\nu}}, \quad (2.20)$$

where i and j are in class S and ν is in R . Group theory and symmetry arguments are then used to derive similarities and vanishing terms and reduce the perturbation expressions to a few constants. By analytically diagonalizing the remaining matrix, the few remaining constants can be determined by comparing analytical dispersion expressions to experimentally determined effective masses. An important note here is that E_i denotes the energy of band i such that the renormalization of the matrix element depends on the result of the eigenvalue calculation, actually requiring self-consistency. In

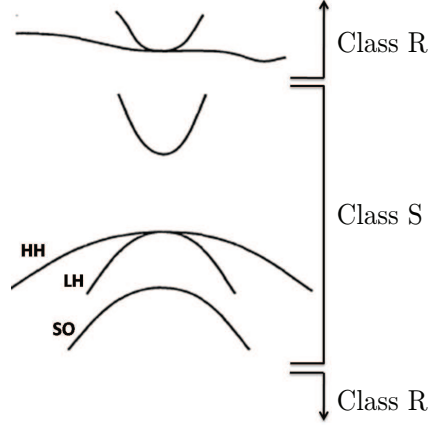


Figure 2.2: Schematic band structure classification in the Löwdin perturbation theory.

practice, the energies E_i are approximated by the zone-center energy $E_i(0)$, given by the matrix element h_{ii} , which is fine close the zone-center. By keeping only one single band in class S , one obtains the single band effective mass dispersion for band i as

$$E_i(0) + \left(\frac{\hbar^2 k^2}{2m_0} + \frac{\hbar}{m_0} \sum_{\nu}^R \frac{\mathbf{k} \cdot \mathbf{p}_{s\nu} \mathbf{p}_{\nu s} \cdot \mathbf{k}}{E_i - h_{\nu\nu}} \right) = E_i(0) + \frac{\hbar^2}{2} \mathbf{k}^T \frac{1}{\mathbf{m}^*} \mathbf{k}. \quad (2.21)$$

In the case of several bands within the class S , the resulting matrix can be written, ordered by the dependence on the wavenumber \mathbf{k} , as

$$\sum_{i,j=x,y,z} \mathbf{H}_{i,j}^{(2)} k_i k_j + \sum_{i=x,y,z} \mathbf{H}_{i,j}^{(1)} k_i + \mathbf{H}^{(0)}. \quad (2.22)$$

To summarize, the second order terms $\mathbf{H}_{i,j}^{(2)}$ are a result of the combination of the free carrier dispersion and the perturbation treatment of remote states in class R , while first order terms $\mathbf{H}_{i,j}^{(1)}$ stem from the direct treatment of the $\mathbf{k} \cdot \mathbf{p}$ interaction (and later from linear spin-orbit terms), while zero order terms $\mathbf{H}^{(0)}$, contain zone-center energies (and possible terms if the zone-center basis is not orthogonal).

2.2 The $\mathbf{k} \cdot \mathbf{p}$ Envelope Function Method

2.2.1 Introduction

In previous sections, the crystal was assumed to be homogeneous and infinitely extended. In nanostructures, this assumption is no longer valid and the translational symmetry is broken in certain directions. As a consequence, a carrier might be energetically confined within a lower-bandgap material, but still free to propagate within the translational invariant direction. In the case of a quantum well, the symmetry is broken by the atoms of the other species in one direction, for a quantum wire, it is broken in two directions and for a quantum dot in all three directions. Consequently, the number of translational invariant directions is reduced from two for a quantum well to zero for a quantum dot. As a result, the Bloch function employing the plane wave ansatz has to be modified

$$\varphi_{m\mathbf{k}_t}(\mathbf{r}, z) = \sum_n u_n(\mathbf{r}, z) e^{i\mathbf{k}_t \cdot \mathbf{r}} F_{n\mathbf{k},m}(z). \quad (2.23)$$

Here, \mathbf{r} denotes the coordinate of translational invariant direction(s), z is the coordinate of the direction(s) where the crystal symmetry is broken and $u_n(\mathbf{r}, z)$ is a lattice-periodic function. The crystal momentum \mathbf{k} is only defined within the translational invariant direction. The expression $F_{n\mathbf{k},m}(z)$ is referred to as slowly-varying envelope and denotes at every position in the symmetry broken direction z , how the lattice-periodic functions are mixed together. In the bulk crystal, the plane wave term decouples the wavefunctions with different crystal momenta \mathbf{k} . In a nanostructure, this decoupling is only true for the translational invariant direction, while in the symmetry broken direction, the states are now mixed together.

As a result of the symmetry breaking, the bands are split into *subbands*, depending on the transversal crystal momentum \mathbf{k}_t . The task of the envelope function method is now to select a suitable set of lattice periodic functions $u_n(\mathbf{r}, z)$ for 2.23 and derive a proper equation to determine the envelopes $F_{n\mathbf{k},m}(z)$.

2.2.2 $\mathbf{k} \cdot \mathbf{p}$ Envelope Function Ansatz

The traditional ansatz is to use the zone-center $\mathbf{k} \cdot \mathbf{p}$ lattice periodic functions $u_{n0}(\mathbf{r})$ for the expansion 2.23, together with a set of matching conditions. The equation for the envelopes is obtained by replacing the wave number k_i by the corresponding operator $-i\partial_i$. As in the nanostructure, different materials are involved, the wavefunction is in each material expanded into the materials zone-center functions. The result is that the effective mass like parameters from the perturbation interaction with remote states and the zone-center energies are position dependent. For the single-band effective mass approximation for e.g. the conduction band in a quantum well for $\mathbf{k}_t = 0$, the envelope equation is given by

$$\left(-\frac{\hbar^2}{2m^*(z)} \frac{\partial^2}{\partial z^2} + E_c(z) \right) F_s(z) = E(0)F_s(z). \quad (2.24)$$

$E_c(z)$ denotes the position dependent bulk band edge, corresponding in the direct band gap semiconductors to the conduction band energy at Γ . Once the eigenvalues $E_m(0)$ and normalized eigenfunctions $F_{s,m}(z)$ (indexed by the subband quantum number m) of 2.24 are obtained, the in-plane dispersion is usually approximated using the dominant effective mass of the quantum well material

$$E_m(\mathbf{k}) = E_m(0) + \frac{\hbar^2 k^2}{2m_c^*}. \quad (2.25)$$

The way the equation is written, it is in the presence of a material interface not Hermitian and therefore unexpected imaginary eigenvalues for the energy would result. The usual ad-hoc fix, justified by the requirement of a continuous probability flow, is to rewrite the second order differential operator (**author?**) [15]

$$-\frac{\hbar^2}{2m^*(z)} \nabla^2 \rightarrow -\nabla \frac{\hbar^2}{2m^*(z)} \nabla. \quad (2.26)$$

The particular order of the coefficient and the differential operators is commonly referred to as operator ordering. The form of 2.26 is denoted as Ben-Daniel and Duke ordering (**author?**) [5], but within the single-band effective mass theory, other orderings are suggested too (see (**author?**))

[36] and references therein). The ordering is irrelevant within bulk materials, but plays a substantial role at a material interface: it is equivalent to the matching conditions for the bulk Bloch functions. In the case of a multi-band equation, where not only one, but several lattice periodic functions are included, one obtains in analogy to 2.26 for all envelopes involved $\mathbf{F}(z) = (F_1(z), F_2(z), \dots, F_M(z))^T$ a system of coupled partial differential equations

$$\mathbf{H}_{\mathbf{k}\cdot\mathbf{p}}(z)\mathbf{F}(z) = E\mathbf{F}(z), \quad (2.27)$$

where the $\mathbf{k} \cdot \mathbf{p}$ differential operator is given by

$$\begin{aligned} \mathbf{H}_{\mathbf{k}\cdot\mathbf{p}}(z) = & - \sum_{i,j} \partial_i \mathbf{H}_{i,j}^{(2)}(\mathbf{r}; \mathbf{k}_t) \partial_j \\ & + \sum_i \left(\mathbf{H}_{i,L}^{(1)}(\mathbf{r}; \mathbf{k}_t) \partial_i + \partial_i \mathbf{H}_{i,R}^{(1)}(\mathbf{r}; \mathbf{k}_t) \right) \\ & + \mathbf{H}^{(0)}(\mathbf{r}; \mathbf{k}_t). \end{aligned} \quad (2.28)$$

Here the Hermitian operator ordering has already been introduced. The problem is that within the bulk $\mathbf{k} \cdot \mathbf{p}$ Hamiltonian, terms of the type $Nk_i k_j$ with $i \neq j$ can appear, for which the operator ordering is not clear. The usual fix is to split the contribution symmetrically

$$Nk_i k_j \rightarrow \partial_i \frac{N}{2} \partial_j - \partial_j \frac{N}{2} \partial_i. \quad (2.29)$$

It can be shown that this particular choice, which is called *symmetrized operator ordering*, may lead to erroneous results. The traditional envelope equations for one and several bands are widely applied and used in a variety of numerical calculations of quantum wells (and superlattices) (**author?**) [1, 3, 4, 20, 16].

Beside its successful application to some material systems, the traditional way of deriving the envelope equations contains several ad hoc fixes, which are required within the presence of material interfaces. The operator ordering is crucial at a material interface, where the material parameters change and therefore the ad-hoc operator ordering involves unknown approxima-

tions made to the effect of the interface. In order to analyze the involved approximations, Burt (**author?**) [10, 12, 9, 8] derived the operator ordering 2.26 from the nanostructure's Schrödinger equation and demonstrated that the symmetrization approach for the terms 2.29 in the multi-band envelope equation is incorrect. The derived multi-band Hamiltonian is Hermitian, but not necessarily symmetric. The derivation focusing on operator ordering is not summarized here, but the reader is referred to reviews (**author?**) [9, 12] and for the numerical estimates of the introduced errors to (**author?**) [10]. In essence, Burt's theory clearly demonstrated the existence and omission of interface terms and showed that exact envelope equations could be derived from the original Schrödinger equation. But Burt's theory is not widely applied. The issue of operator ordering attracts growing interest and it is crucial for the mathematical stability of the envelope equations (**author?**) [42?]. Foreman (**author?**) [21] derived the correct operator ordering for zinc-blende crystals and therefore the derived operator ordering is commonly referred to as Burt-Foreman operator ordering. Beside the operator ordering, the theory regarding the omitted interface terms in the traditional model is only used rarely (**author?**) [23, 22]. The effect of the interface terms is to perturb the system and create an additional mixing of the bands. In the traditional envelope equations, the effect of the interface was introduced using phenomenological models (see e.g. (**author?**) [31] and references therein) or by a variational least action principle (**author?**) [39]. The reason of the fundamental popularity of the traditional envelope function method over Burt's method is given by its simple form, which allows to write quantum well solvers within days, and the fact that mostly known, bulk input parameters can be used, which is not the case for the interface terms within the exact envelope function theory.

2.2.3 The Zinc-blende Models

2.2.3.1 Direct Interaction

To apply the envelope equations 2.27 to direct-bandgap semiconductor nanostructures, the exact form of the $\mathbf{k} \cdot \mathbf{p}$ Hamiltonian at the Γ point is required.

Ignoring spin, the top of the valence band at Γ is triply degenerate, corresponding to the Γ_{15} representation with p -type basis functions x, y and z , while the lowest-lying conduction band is of s -type symmetry, corresponding to Γ_1 . The direct interaction terms 2.18 of the $\mathbf{k} \cdot \mathbf{p}$ matrix for s, x, y and z are given by (author?) [28]

$$\mathbf{H}_d^{4 \times 4} = \begin{pmatrix} & |s\rangle & |x\rangle & |y\rangle & |z\rangle \\ \hline |s\rangle & E_c + \frac{\hbar^2}{2m_0} & iPk_x & iPk_y & iPk_z \\ |x\rangle & -ik_x P & E_v + \frac{\hbar^2}{2m_0} & 0 & 0 \\ |y\rangle & -ik_y P & 0 & E_v + \frac{\hbar^2}{2m_0} & 0 \\ |z\rangle & -ik_z P & 0 & 0 & E_v + \frac{\hbar^2}{2m_0} \end{pmatrix}. \quad (2.30)$$

Here, E_c and E_v correspond to the zone-center energies

$$E_c = \langle s|H|s\rangle \quad (2.31)$$

$$E_v = \langle x|H|x\rangle \quad (2.32)$$

$$P = -\frac{i\hbar}{m_0} \langle s|p_x|s\rangle \quad (2.33)$$

and P the nonzero interband momentum matrix element from the direct $\mathbf{k} \cdot \mathbf{p}$ interaction between the conduction- and the valence band. The momentum matrix element is often given as an energy parameter E_p , the *optical matrix parameter*, related to P by

$$E_p = \frac{2m_0}{\hbar^2} P^2. \quad (2.34)$$

For the Γ_{15} states, the nonzero momentum matrix element is of the type $\langle x|p_y|z\rangle$, where no coordinate appears twice (author?) [43] (the crystal is invariant under a rotation of 180° around one of the axes like (author?) [38]). Therefore, one would expect the direct interaction within the valence band $\mathbf{k} \cdot \langle x|\mathbf{p}|y\rangle$ resulting into a linear term in \mathbf{k} given explicitly by $k_z \langle x|p_z|y\rangle$. In fact, the first order matrix elements within Γ_{15} vanish due to time reversal symmetry of the Hamiltonian (author?) [17]. For example, a reflection in the (110) plane for $\langle x^a|p_z|y^b\rangle$ results in $\langle y^a|p_z|x^b\rangle$, while integration by parts

gives $\langle x^a | p_z | y^b \rangle = -\langle y^b | p_z | x^a \rangle$. Here a and b index the degenerate level. If the states are from the same degenerate level, then $a = b$ and the matrix elements vanish. If the states are not from the same degenerate level, the interaction is nonzero.

The operator ordering in the first order terms, e.g. $H_{sx} = iPk_x$ and $H_{xs} = -ik_xP$ is an ad hoc fix. If P is allowed to vary, the here chosen ordering is required to ensure the Hamiltonians Hermiticity.

2.2.3.2 Remote Contributions

The next step is to include the interaction between the remote states and keep track of the correct operator ordering. It is clear from table 2.1 that the remote contributions to the conduction band stem from remote Γ_{15} states, while the valence band states have contributions from all except the Γ_2 states. The corresponding terms are given by the matrix $\mathbf{H}_r^{4 \times 4}$ 2.37 and the coefficients 2.38. In deriving these terms, the energy for the energy-dependent renormalization has been replaced by the according band edge energies E_v and E_c . Although the approximation might be reasonable for very remote bands ν , it remains crude. The derivation of the terms these terms involves only symmetry arguments similar to the already used arguments within this chapter. The bar in \bar{A}_c , \bar{L} and \bar{M} indicates the close relationship to the parameters \tilde{A}_c, \tilde{L}' and \tilde{M} , which include the free-electron dispersion

$$\tilde{A}_c = \bar{A}_c + \frac{\hbar^2}{2m_0}, \quad \tilde{L}' = \bar{L} + \frac{\hbar^2}{2m_0}, \quad \tilde{M} = \bar{M} + \frac{\hbar^2}{2m_0}, \quad (2.35)$$

whereas in this case the free electron dispersion is still contained in the direct interaction matrix 2.30. The operator ordering in the offdiagonal terms $k_y \tilde{N}_+ k_x + k_x \tilde{N}_- k_y$ has been derived by Foreman 22. The term \tilde{N}_+ contains the contribution from $\Gamma_1 (F)$ and $\Gamma_{12} (G)$ bands, while \tilde{N}_- contains the contributions from $\Gamma_{15} (H_1)$ and $\Gamma_{25} (H_2)$ bands. In the bulk $\mathbf{k} \cdot \mathbf{p}$ theory, the ordering is irrelevant and the terms are summed together into the Kane's parameter \tilde{N}'

$$\tilde{N}' = \tilde{N}_+ + \tilde{N}_-. \quad (2.36)$$

Within the traditional $\mathbf{k} \cdot \mathbf{p}$ envelope function method applied to heterostructure, the symmetrized operator ordering 2.29 simply uses

$$\tilde{N}_+ = \tilde{N}_- = \frac{\tilde{N}'}{2}.$$

The parameters \tilde{L}' , \tilde{M} and \tilde{N} are usually determined by calculating analytical expressions for the dispersion and relating them to measured effective masses. The detailed splitting of \tilde{N}' into \tilde{N}_+ and \tilde{N}_- is not directly accessible from experiment, but can be estimated (**author?**) [21] using the following arguments: The term \tilde{N}_- contains contributions of Γ_{15} and Γ_{25} bands. The Γ_{25} bands can only be formed by f -type and higher atomic orbitals, while Γ_{15} bands can be formed by p -, d -, f - and higher type orbitals (**author?**) [22]. Within the usual semiconductors, the influence of f orbitals is insignificant. Therefore, neglecting the influence of the Γ_{25} bands ($H_2 = 0$) and using 2.38, the value for \tilde{N}_- is given by

$$\tilde{N}_- = \bar{M} = \tilde{M} - \frac{\hbar^2}{2m_o}.$$

\tilde{N}_+ can be deduced using 2.36 and the experimentally determined value for \tilde{N}' . In a usual zinc-blende semiconductor such as $GaAs$, $\tilde{M} = -2.65$ and $\tilde{N}' = -17.4$ (in units of $\frac{\hbar^2}{2m_0}$). The symmetric operator ordering would therefore use $\tilde{N}_{+/-} = -8.7$, while the Burt-Foreman ordering gives strongly asymmetric values $\tilde{N}_+ = -13.75$ and $\tilde{N}_- = -3.65$. In contrast to the operator ordering within the valence band, the ordering in the off-diagonal terms between the conduction and valence bands, given by the terms $k_y C k_z + k_z C k_y$, is required to be symmetric. Only remote Γ_{15} type bands mix into the s -type conduction band, and therefore, the non-vanishing elements from the perturbation are

$$k_y \langle s | p_y | y^r \rangle \langle y^r | p_z | x \rangle k_z + k_z \langle s | p_z | y^r \rangle \langle z^r | p_y | x \rangle k_y.$$

By crystal symmetry, these terms are equal. The term C is related to the common Kane parameter $B = 2C$. As B is usually small, it is commonly

neglected, i.e. $C = 0$.

$$\mathbf{H}_r^{4 \times 4} = \begin{pmatrix} & |s\rangle & |x\rangle & |y\rangle \\ |s\rangle & k\bar{A}_c k & k_y C k_z + k_z C k_y & k_x C k_z + k_z C k_x & k_y C \\ |x\rangle & k_z C k_y + k_y C k_z & k_x \bar{L} k_x + k_y \bar{M} k_y + k_z \bar{M} k_z & k_x \tilde{N}_+ k_y + k_y \tilde{N}_- k_x & k_x \tilde{N}_+ \\ |y\rangle & k_z C k_x + k_x C k_z & k_y \tilde{N}_+ k_x + k_x \tilde{N}_- k_y & k_y \bar{L} k_y + k_x \bar{M} k_x + k_z \bar{M} k_z & k_y \tilde{N}_+ \\ |z\rangle & k_x C k_y + k_y C k_x & k_z \tilde{N}_+ k_x + k_x \tilde{N}_- k_z & k_z \tilde{N}_+ k_y + k_y \tilde{N}_- k_z & k_z \bar{L} k_z + k_y \tilde{N}_+ \end{pmatrix} \quad (2.37)$$

$$\begin{aligned} \bar{L} &= F + 2G, \\ \bar{M} &= H_1 + H_2, \\ \tilde{N}_+ &= F - G, \\ \tilde{N}_- &= H_1 - H_2, \\ F &= \frac{\hbar^2}{m_0^2} \sum_{\nu}^{\Gamma_1} \frac{|\langle x | p_x | u_{\nu} \rangle|^2}{(E_v - E_{\nu})}, \\ G &= \frac{\hbar^2}{m_0^2} \sum_{\nu}^{\Gamma_{12}} \frac{|\langle x | p_x | u_{\nu} \rangle|^2}{(E_v - E_{\nu})}, \\ H_1 &= \frac{\hbar^2}{m_0^2} \sum_{\nu}^{\Gamma_{15}} \frac{|\langle s | p_x | u_{\nu} \rangle|^2}{(E_c - E_{\nu})}, \\ H_2 &= \frac{\hbar^2}{m_0^2} \sum_{\nu}^{\Gamma_{25}} \frac{|\langle x | p_x | u_{\nu} \rangle|^2}{(E_v - E_{\nu})}, \\ \bar{A}_c &= \frac{\hbar^2}{m_0^2} \sum_{\nu}^{\Gamma_{15}} \frac{|\langle s | p_x | u_{\nu} \rangle|^2}{(E_c - E_{\nu})}, \\ C &= \frac{\hbar^2}{m_0^2} \sum_{\nu}^{\Gamma_{15}} \frac{\langle s | p_x | u_{\nu} \rangle \langle u_{\nu} | p_x | z \rangle}{(\frac{1}{2}(E_c + E_v) - E_{\nu})}. \end{aligned} \quad (2.38)$$

2.2.3.3 Spin-Orbit Interaction

Up to this point, the electron spin has been omitted. Within the semiconductors involving heavier atoms, the spin-orbit interaction has a large impact on the electron dispersions. The spin-orbit energy leads to additional terms

in the equation 2.24 for the zone-center functions, namely

$$H_{SO,\mathbf{p}} = \frac{\hbar}{4m_0^2c^2} (\nabla V \times \mathbf{p}) \cdot \boldsymbol{\sigma}, \quad (2.39)$$

$$H_{SO,\mathbf{k}} = \frac{\hbar}{4m_0^2c^2} (\nabla V \times \mathbf{k}) \cdot \boldsymbol{\sigma}, \quad (2.40)$$

where c is the vacuum speed of light and $\boldsymbol{\sigma}$ are the *Pauli operators* acting on the electron-spin variable

$$\sigma_x = \begin{pmatrix} 0 & 1 \\ 1 & 0 \end{pmatrix}, \quad \sigma_y = \begin{pmatrix} 0 & -i \\ i & 0 \end{pmatrix}, \quad \sigma_z = \begin{pmatrix} 1 & 0 \\ 0 & -1 \end{pmatrix}.$$

The Bloch basis functions have to be extended to include the spin degree of freedom, which is done by giving the spin z -component, which can be either up $|\uparrow\rangle$ or down $|\downarrow\rangle$. The spin variable is diagonal, meaning that $\langle\uparrow|\uparrow\rangle = \langle\downarrow|\downarrow\rangle = 1$ and $\langle\uparrow|\downarrow\rangle = 0$. Using the spin, the initial basis of four states describing the lowest conduction band and the top valence bands is doubled to eight states

$$|s\uparrow\rangle, |x\uparrow\rangle, |y\uparrow\rangle, |z\uparrow\rangle, |s\downarrow\rangle, |x\downarrow\rangle, |y\downarrow\rangle, |z\downarrow\rangle. \quad (2.41)$$

All operators in the zone-center Hamiltonian 2.14 do not act on the spin variable. Therefore, the Hamiltonian is diagonal in the spin variable. Within the basis 2.41, the Hamiltonian is given by

$$\mathbf{H}_{rd}^{8 \times 8} = \begin{pmatrix} \mathbf{H}_d^{4 \times 4} + \mathbf{H}_r^{4 \times 4} & 0 \\ 0 & \mathbf{H}_d^{4 \times 4} + \mathbf{H}_r^{4 \times 4} \end{pmatrix}. \quad (2.42)$$

In contrast to this Hamiltonian, the spin-orbit interaction 2.39 and 2.40 is not diagonal in the basis 2.41. The reason to this lies in the symmetry of the spin. The crystal potential $V(\mathbf{r})$ without spin terms is invariant under any rotation around an angle of 2π , denoted here as \hat{E} . Under such a rotation, the wavefunction including the spin switches sign and is only invariant under the rotation of 4π . Therefore, if the point group of the crystal neglecting spin is given by \mathcal{G} , then the point group including spin will be given by the

elements of \mathcal{G} and $\hat{E}\mathcal{G}$, leading to the definition of the *double-group* $\tilde{\mathcal{G}}$ of \mathcal{G} defined as

$$\tilde{\mathcal{G}} = \{g, \tilde{g} = -g\} \quad \forall g \in \mathcal{G}.$$

The spin-orbit interaction for $H_{SO,\mathbf{p}}$ of 2.39 leads, for the basis in 2.41, to **(author?)** [18]

$$\mathbf{H}_{SO,\mathbf{p}} = \frac{\Delta}{3} \begin{pmatrix} 0 & 0 & 0 & 0 & 0 & 0 & 0 & 0 \\ 0 & 0 & -i & 0 & 0 & 0 & 0 & 1 \\ 0 & i & 0 & 0 & 0 & 0 & 0 & -i \\ 0 & 0 & 0 & 0 & 0 & -1 & i & 0 \\ 0 & 0 & 0 & 0 & 0 & 0 & 0 & 0 \\ 0 & 0 & 0 & -1 & 0 & 0 & i & 0 \\ 0 & 0 & 0 & -i & 0 & -i & 0 & 0 \\ 0 & 1 & i & 0 & 0 & 0 & 0 & 0 \end{pmatrix}. \quad (2.43)$$

Here, the spin-orbit energy Δ is defined as

$$\Delta = -3i \frac{\hbar}{4m_0^2 c^2} \left\langle x \mid (\nabla V \times \mathbf{p})_y \mid z \right\rangle.$$

The k -dependent spin-orbit interaction $H_{SO,\mathbf{k}}$ of 2.40 is small and therefore commonly neglected **(author?)** [28]. The result of $H_{SO,\mathbf{k}}$ are terms linear in k , leading to an off-diagonal coupling between the conduction and the valence band. Further, the spin-orbit interaction $H_{SO,\mathbf{p}}$ is usually only included in the direct interaction, while perturbative contributions from remote bands are in general neglected. The effect of the spin-orbit interaction is to split the six-fold (threefold without spin) degeneracy of the valence band at Γ into a fourfold degeneracy with eigenvalue $\frac{\Delta}{3}$ and a two-fold degeneracy with an eigenvalue of $-\frac{2\Delta}{3}$. In other words, the states are separated by Δ . The four-fold degenerate states corresponds to the irreducible representation Γ_8 of the double group of T_d . Away from Γ , these states create the *heavy-hole* (HH) and the *light-hole* (LH) bands. The two-fold degenerate states correspond to the Γ_7 representation and lie below the Γ_8 states by $-\Delta$. The Γ_7 band is referred to as *spin-orbit split off band* (SO). The lowest conduction band

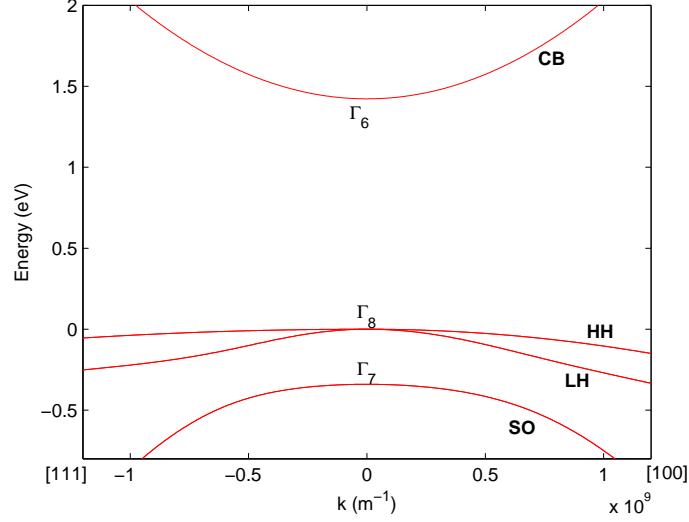


Figure 2.3: Band structure of bulk *GaAs* around the Γ point at room temperature, calculated using the $8 \times 8 \mathbf{k} \cdot \mathbf{p}$ for two crystal directions.

(CB) states finally correspond to Γ_6 states. The situation is illustrated in Fig. 2.3, where the band structure of *GaAs* calculated using the here presented $\mathbf{k} \cdot \mathbf{p}$ model is plotted around $\mathbf{k} = 0$. The experimental accessible bandgap is given by the difference between the Γ_6 and the Γ_8 states. Therefore, the valence band edge E_v in 2.32, needs to be shifted by $-\frac{\Delta}{3}$.

The here elaborated model, including the CB, HH, LH and SO band, is commonly referred to as the $8 \times 8 \mathbf{k} \cdot \mathbf{p}$ model. For large band gap materials, the coupling between the conduction and valence bands is weak and therefore the $8 \times 8 \mathbf{k} \cdot \mathbf{p}$ model can be divided into to a 6×6 model, including only the valence bands and a single band model for the spin degenerate conduction band. This division is achieved by perturbatively folding the conduction band onto the valence bands and vice versa. The $6 \times 6 \mathbf{k} \cdot \mathbf{p}$ is therefore obtained by using only the valence band part of $\mathbf{H}_{rd}^{8 \times 8} + \mathbf{H}_{SO, \mathbf{p}}$ with modified parameters L' and N' given by

$$L' = \tilde{L}' + \frac{P^2}{E_g}, \quad N_+ = \tilde{N}_+ + \frac{P^2}{E_g} \quad (2.44)$$

instead of \tilde{L}' and \tilde{N}_+ . The parameter \tilde{M} , and consequently \tilde{N}_- , remain unch-

nged. Thereby, the correct operator ordering is conserved. The conduction band parameter is obtained using

$$A_c = \tilde{A}_c + \frac{P^2}{E_g}, \quad (2.45)$$

which is then equal to the common conduction band effective mass. For some semiconductors, the spin-orbit splitting is large and the SO band has only little influence on the top of the valence band. Then, the $6 \times 6 \mathbf{k} \cdot \mathbf{p}$ model can be further reduced to only include the HH and LH bands. The reduction is performed by choosing a combination of basis functions 2.41 effectively diagonalizing the spin-orbit interaction $\mathbf{H}_{SO, \mathbf{p}}$. The new basis is labelled according to its total angular momentum J and the angular momentum around the z -axis, J_z . A possible choice, using $|J, J_z\rangle$ as notation, is given by

$$\begin{aligned} u_{hh} &= \left| \frac{3}{2}, \frac{3}{2} \right\rangle = -\frac{1}{\sqrt{2}} (|x \uparrow\rangle + i |y \uparrow\rangle), \\ u_{lh} &= \left| \frac{3}{2}, \frac{1}{2} \right\rangle = -\frac{1}{\sqrt{6}} (|x \downarrow\rangle + i |y \uparrow\rangle) + \sqrt{\frac{2}{3}} |z \uparrow\rangle, \\ \bar{u}_{lh} &= \left| \frac{3}{2}, -\frac{1}{2} \right\rangle = \frac{1}{\sqrt{6}} (|x \uparrow\rangle - i |y \uparrow\rangle) + \sqrt{\frac{2}{3}} |z \downarrow\rangle, \\ \bar{u}_{hh} &= \left| \frac{3}{2}, -\frac{3}{2} \right\rangle = \frac{1}{\sqrt{2}} (|x \downarrow\rangle - i |y \downarrow\rangle), \\ u_{SO} &= \left| \frac{1}{2}, \frac{1}{2} \right\rangle = \frac{1}{\sqrt{3}} (|x \downarrow\rangle + i |y \downarrow\rangle + |z \uparrow\rangle), \\ \bar{u}_{SO} &= \left| \frac{1}{2}, -\frac{1}{2} \right\rangle = \frac{1}{\sqrt{3}} (|x \uparrow\rangle - i |y \uparrow\rangle - |z \downarrow\rangle). \end{aligned} \quad (2.46)$$

The four states with total angular momentum of $\frac{3}{2}$ belong to Γ_8 and the two states with an angular momentum of $\frac{1}{2}$ form the Γ_7 (or SO) bands. Transforming the Hamiltonian into the basis 2.46 and neglecting the Γ_7 rows and columns finally results in the $4 \times 4 \mathbf{k} \cdot \mathbf{p}$ model. Within the $4 \times 4 \mathbf{k} \cdot \mathbf{p}$ model, it is common to use the Luttinger parameters γ_1, γ_2 and γ_3 ²(**author?**)

²The full listing of these parameters is given in Appendix XXX .

[33] instead of the Kane's parameters of the 6×6 model L' , M and N' . The Luttinger parameters are usually those given in literature. The parameters are related to each other via

$$\begin{aligned} L' &= -\frac{\hbar^2}{2m_0} (\gamma_1 + 4\gamma_2) \\ M &= -\frac{\hbar^2}{2m_0} (\gamma_1 - 2\gamma_2) \\ N' &= -\frac{\hbar^2}{2m_0} 6\gamma_3. \end{aligned} \quad (2.47)$$

From 2.47, the parameters for 8×8 model can be calculated using the renormalization 2.44.

In terms of the Luttinger parameters the full 8×8 Hamiltonian can be written explicitly as (**author?**) [15, 34, 33]

$$\mathbf{H}^{8 \times 8} = \begin{pmatrix} E_c & P_z & \sqrt{2}P_z & -\sqrt{3}P_+ & 0 & \sqrt{2}P_- & P_- & 0 \\ P_z^\dagger & P + \Delta & \sqrt{2}Q^\dagger & -S^\dagger/\sqrt{2} & -\sqrt{2}P_+^\dagger & 0 & -\sqrt{3/2}S & -\sqrt{2}R \\ \sqrt{2}P_z^\dagger & \sqrt{2}Q & P - Q & -S^\dagger & -P_+^\dagger & \sqrt{3/2}S & 0 & R \\ -\sqrt{3}P_+^\dagger & -S/\sqrt{2} & -S & P + Q & 0 & \sqrt{2}R & R & 0 \\ 0 & -\sqrt{2}P_+ & -P_+ & 0 & E_c & P_z & -\sqrt{2}P_z & -\sqrt{3}P_- \\ \sqrt{2}P_-^\dagger & 0 & \sqrt{3/2}S^\dagger & \sqrt{2}R^\dagger & P_z^\dagger & P + \Delta & \sqrt{2}Q^\dagger & -S/\sqrt{2} \\ P_-^\dagger & -\sqrt{3/2}S^\dagger & 0 & R^\dagger & -\sqrt{2}P_z^\dagger & \sqrt{2}Q & P - Q & S \\ 0 & -\sqrt{2}R^\dagger & R^\dagger & 0 & -\sqrt{3}P_-^\dagger & -S^\dagger/\sqrt{2} & S^\dagger & P + Q \end{pmatrix} \quad (2.48)$$

where

$$E_c = E_g + \frac{\hbar^2}{2m_0} (k_x^2 + k_y^2 + k_z^2), \quad (2.49)$$

$$P = \frac{\hbar^2}{2m_0} \gamma_1 (k_x^2 + k_y^2 + k_z^2), \quad (2.50)$$

$$P_{\pm} = \sqrt{\frac{1}{6}} [i\mathcal{P} (k_x \pm ik_y) + \mathcal{B}k_z (k_y \pm ik_x)] \quad (2.51)$$

$$P_z = \sqrt{\frac{1}{3}} (i\mathcal{P}k_z + \mathcal{B}k_xk_y), \quad (2.52)$$

$$Q = \frac{\hbar^2}{2m_0} \gamma_2 (k_x^2 + k_y^2 - 2k_z^2), \quad (2.53)$$

$$R = \frac{\hbar^2}{2m_0} [-\sqrt{3}\gamma_2 (k_x^2 - k_y^2) + i2\sqrt{3}\gamma_3 k_xk_y], \quad (2.54)$$

$$S = \frac{\hbar^2}{2m_0} \gamma_3 (k_x - ik_y) k_z. \quad (2.55)$$

The parameter Δ is, as before, the spin-orbit splitting energy. The coupling between the Γ conduction band edge state $|s\rangle$ and the Γ valence band edge state $|z\rangle$ is given by

$$\mathcal{P} = -\frac{\hbar^2}{m_0} \int_{V_c} \varphi_s \frac{\partial}{\partial z} \varphi_z. \quad (2.56)$$

The Kane parameter \mathcal{B} describes the inversion asymmetry. In most practical calculations, this parameter is neglected. The parameters $\gamma_1, \gamma_2, \gamma_3$ and \mathcal{P} can be determined from effective masses at the Γ point of the bulk semiconductor (author?) [15]

$$\frac{m_0}{m_{hh}(001)} = \gamma_1 - 2\gamma_2, \quad (2.57)$$

$$\frac{m_0}{m_{lh}(001)} = \gamma_1 + 2\gamma_2 + \lambda, \quad (2.58)$$

$$\frac{m_0}{m_{SO}(001)} = \gamma_1 + \frac{1}{2}\lambda r, \quad (2.59)$$

$$\frac{m_0}{m_{hh}(111)} = \gamma_1 - 2\gamma_3, \quad (2.60)$$

where the dimensionless parameters λ and r are given by

$$\lambda = \frac{4m_0\mathcal{P}^2}{3\hbar^2 E_g}, \quad (2.61)$$

$$r = \frac{E_g}{E_g + \Delta}. \quad (2.62)$$

Put here the 6X6 and 4X4 Hamiltonians

2.2.4 Two Band Model

The conduction band can be modeled quite easily if we assume that the interaction with the other bands is weak enough for it to be treated perturbatively, i.e. use a simple effective mass model. In the case of the valence band, however, the strong interaction between the degenerate light and heavy hole bands (near the band edge) requires that these bands are taken into account explicitly. Only when we consider energy levels deep into the valence bands (close to the SO splitting energy, about 300 meV in *GaAs*) do the coupling terms to the SO and conduction bands (1.5 eV splitting) can be introduced through the effective mass.

The degeneracy of the light and heavy hole bands near the band edge generates a coupling term (as in the Luttinger Hamiltonian). Including spin degeneracy, this yields a set of four coupled effective mass equations (**author?**) [15, 2, 7].

Fortunately, this set of coupled equations can be greatly simplified by a method described in (**author?**) [7]. Here a unitary transformation of the four basis Bloch functions in 2.46 into a new set u_A, u_B, u_C, u_D to decouple the set of four coupled equations into two coupled ones. The Bloch functions

u_i are given by

$$u_A = \frac{1}{\sqrt{2}} (u_{hh} - \bar{u}_{hh}), \quad (2.63)$$

$$u_B = \frac{1}{\sqrt{2}} (-u_{lh} - \bar{u}_{lh}), \quad (2.64)$$

$$u_C = \frac{1}{\sqrt{2}} (u_{lh} + \bar{u}_{lh}), \quad (2.65)$$

$$u_D = \frac{1}{\sqrt{2}} (u_{hh} + \bar{u}_{hh}). \quad (2.66)$$

Consequently, the 4×4 $\mathbf{k} \cdot \mathbf{p}$ Hamiltonian

$$\mathbf{H}^{4 \times 4} = \begin{pmatrix} P - Q & -S^\dagger & 0 & R \\ -S & P + Q & R & 0 \\ 0 & R^\dagger & P - Q & S \\ R^\dagger & 0 & S^\dagger & P + Q \end{pmatrix}. \quad (2.67)$$

In terms of the the new base proposed above, it can be diagonalized into two 2×2 block matrices, upper H^U and lower H^L , given by

$$H^\sigma = \begin{pmatrix} P \pm Q & W \\ W^\dagger & P \mp Q \end{pmatrix}, \quad (2.68)$$

where $W = |R| - i|S|$. The index $\sigma = U(L)$ refers to the upper (lower) \pm signs. The upper and lower blocks are equivalent, showing the double degeneracy of the heavy and light hole bands. It is therefore sufficient to solve the upper block and obtain its solutions. The solutions of the lower block can easily be determined from the latter.

We can identify $P - Q$ and $P + Q$ with the light hole energy (operator) \hat{H}_{lh} and the heavy hole energy \hat{H}_{hh} , respectively. Similarly to the conduction band case, the Schrödinger equation with the Hamiltonian 2.68 can be

simplified into an effective-mass formalism with

$$\hat{H}_{lh} = -(\gamma_1 + 2\gamma_2) \frac{\partial^2}{\partial z^2} + (\gamma_1 - \gamma_2) k_t^2, \quad (2.69)$$

$$\hat{H}_{hh} = -(\gamma_1 - 2\gamma_2) \frac{\partial^2}{\partial z^2} + (\gamma_1 + \gamma_2) k_t^2, \quad (2.70)$$

$$\hat{W} = \begin{cases} \sqrt{3}k_t (\gamma_2 k_t - 2\gamma_3 \frac{\partial}{\partial z}) & \text{for [100]} \\ \sqrt{3}k_t (\gamma_3 k_t - 2\gamma_3 \frac{\partial}{\partial z}) & \text{for [110]} \end{cases} \quad (2.71)$$

Finally, we take into account the potential $V(z)$, which represents the (bulk) valence-band-edge offset with respect to an arbitrary reference energy. This allows us write the effective mass equation as

$$\begin{pmatrix} \hat{H}_{hh} + V & \hat{W} \\ \hat{W}^\dagger & \hat{H}_{lh} + V \end{pmatrix} \begin{pmatrix} F_{hh} \\ F_{lh} \end{pmatrix} = E(\mathbf{k}) \begin{pmatrix} F_{hh} \\ F_{lh} \end{pmatrix}, \quad (2.72)$$

where F_{hh} and F_{lh} are the envelope functions corresponding to u_A and u_B respectively. Note that in this formalism, hole energies are taken to be positive.

The first step in solving the quantum well problem, is finding the solution in bulk material, where we take V to be a constant V_0 . The value of V_0 will be different in well material and barriers reflecting the different valence band edge offsets. We can now easily solve for the eigenenergies $E(\mathbf{k})$, yielding the bulk energy dispersion relations for the heavy and light hole subbands. We consider the case of a [100] plane, writing the in-plane \mathbf{k} component as k_t

$$E(\mathbf{k}) - V_0 = \gamma_1 (k_z^2 + k_t^2) \pm \sqrt{4\gamma_2^2 (k_z^2 + k_t^2) + 12(\gamma_3^2 - \gamma_2^2) k_z^2 k_t^2}, \quad (2.73)$$

where the plus sign refers to the light hole solution, and the minus to the heavy hole one. This expression can be rewritten to

$$E(\mathbf{k}) = V_0 + \left[\gamma_1 \pm \gamma_2 \sqrt{1 + 3 \frac{\gamma_3^2 - \gamma_2^2}{\gamma_2^2} \frac{k_z^2 k_t^2}{(k_z^2 + k_t^2)^2}} \right] (k_z^2 + k_t^2). \quad (2.74)$$

A similar derivation can be formulated for the [110] crystal planes.

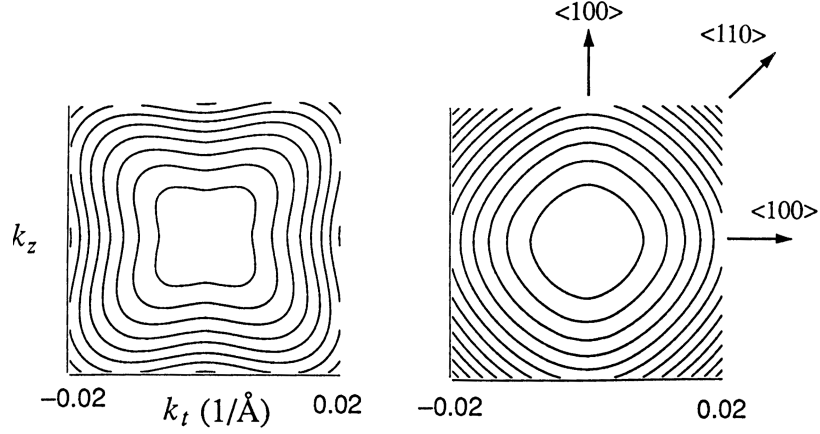


Figure 2.4: Contours of constant energy within any $[100]$ plane of k -space for the heavy (right) and light (left) hole subbands in bulk $GaAs$. The energy spacing between each contour level is 0.5 meV for the HH band and 3 meV for the LH band. The effective HH mass is much larger along the $[110]$ direction than along the $[100]$ direction, as indicated by the larger contour spacing. The effective LH mass is seen to be much more isotropic (after (author?) [44]).

Constant energy contours are shown in Fig. 2.4, illustrating that γ_3 can be related to the mass anisotropy along the $[100]$ and $[110]$ directions. If k_t small compared to k_z , we can expand the square root in 2.73

$$E(\mathbf{k}) = V_0 + (\gamma_1 \pm \gamma_2) (k_z^2 + k_t^2) \pm 3 \frac{\gamma_3^2 - \gamma_2^2}{\gamma_2} k_t^2. \quad (2.75)$$

The Energy term accounting for anisotropy for a given k_t and k_z is equal for the HH and LH subbands. However, due to the lower energy of the HH bands the anisotropy term is relatively more important for HH than for LH, resulting in a clearly anisotropic HH band and a quasi isotropic LH band.

Still, we see that in bulk material, the effective masses along the z -axis $[001]$ and x - and y - axes $[100]$ and $[010]$ are identical (as expected), as the dispersion relation is given by $E(\mathbf{k}) = V_0 + (\gamma_1 \pm 2\gamma_2) k^2$. We can easily find this from 2.73 with $k_t = 0$ for $[001]$, and $k_z = 0$ for the x - and y - directions.

The eigenvectors of 2.72 are found to be, apart from a normalization

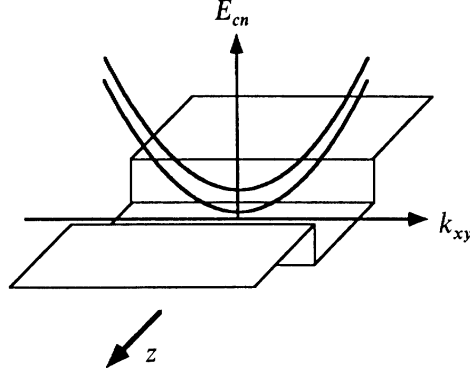


Figure 2.5: The "in-plane" subband structure of the quantum well in the conduction band. Within the plane of the well, the electron still behaves like a "free" electron. Thus, for each quantized level, a parabolic energy subband exist (after (author?) [44]).

constant

$$\varphi_1(\mathbf{k}, \mathbf{r}) = \begin{pmatrix} F_{hh,1} \\ F_{lh,1} \end{pmatrix} = e^{i\mathbf{k}\cdot\mathbf{r}} \begin{pmatrix} H_{lh} + V_0 - E_{hh} \\ -W^\dagger \end{pmatrix}, \quad (2.76)$$

$$\varphi_2(\mathbf{k}, \mathbf{r}) = \begin{pmatrix} F_{hh,2} \\ F_{lh,2} \end{pmatrix} = e^{i\mathbf{k}\cdot\mathbf{r}} \begin{pmatrix} H_{lh} + V_0 - E_{lh} \\ -W^\dagger \end{pmatrix}, \quad (2.77)$$

where the matrix notation implies

$$\varphi = F_{hh}u_A + F_{lh}u_B. \quad (2.78)$$

To solve the quantum well problem, we choose the well growth direction (direction of confinement) along the z -axis. The xy -plane is the plane of the well, as in Fig. 2.5. We can construct a confined solution from the bulk plane wave solutions by imposing boundary conditions along the confinement axis. In the plane of the well, there is no confinement and hence we retain the bulk plane wave solution. By taking a linear combination of the bulk solutions in each material, a general solution can be constructed. As illustrated in Fig. 2.6, four plane wave solutions exist at a given energy, yielding a general

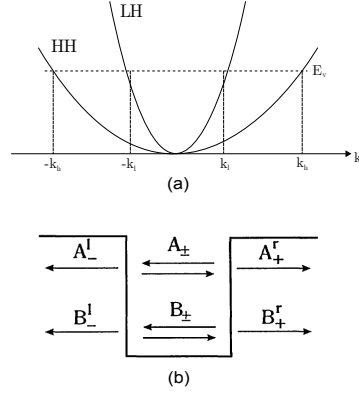


Figure 2.6: At any one energy on a bulk material, we can find four wavevectors corresponding to the heavy and light hole bands. An eigenstate of the Hamiltonian in a quantum well is then made of a linear combination of the bulk plane waves corresponding to those wave vectors. The amplitudes A_\pm and B_\pm in (a) correspond, respectively, to $\pm k_{z1}$ (light hole) and $\pm k_{z2}$ in (b) for the well layer of the quantum well (*GaAs* throughout this thesis). In the barriers (*AlGaAs*) a similar mechanism is employed. The boundary conditions at the interfaces then determine the energy eigenvalues and the coefficients.

solution Φ of the form

$$\Phi = \sum A_\pm \varphi_1(\pm k_{z1}, k_t, \mathbf{r}) + \sum B_\pm \varphi_2(\pm k_{z2}, k_t, \mathbf{r}). \quad (2.79)$$

The four coefficients A_\pm and B_\pm are unknown constants. Both φ_1 and φ_2 are two-component vectors as seen in 2.76 and 2.77. We can write the components of Φ , F_{hh} and F_{lh} , as

$$\begin{aligned} F_{hh} &= e^{i\mathbf{k}_t \cdot \mathbf{r}_t} \left[\sum A_\pm F_{hh,1}(\pm k_{z1}, k_t) e^{\pm i k_{hh} z} + \sum B_\pm F_{hh,2}(\pm k_{z2}, k_t) e^{\pm i k_{lh} z} \right] \quad (2.80) \\ F_{lh} &= e^{i\mathbf{k}_t \cdot \mathbf{r}_t} \left[\sum A_\pm F_{lh,1}(\pm k_{z1}, k_t) e^{\pm i k_{lh} z} + \sum B_\pm F_{lh,2}(\pm k_{z2}, k_t) e^{\pm i k_{hh} z} \right] \quad (2.81) \end{aligned}$$

Thus we have four unknown constants in each region, making a total of 12 unknowns over the three regions. The boundary conditions at the interfaces between the regions and the demand that the solutions be confined in the quantum well provide the necessary relations to solve the problem. In order

to symmetr The following quantities have to be matched across the interfaces

$$F_{hh} \text{ and } (\gamma_1 - 2\gamma_2) \frac{dF_{hh}}{dz} + \sqrt{3}\gamma_3 k_t F_{lh}, \quad (2.82)$$

$$F_{lh} \text{ and } (\gamma_1 - 2\gamma_2) \frac{dF_{lh}}{dz} - \sqrt{3}\gamma_3 k_t F_{hh}. \quad (2.83)$$

These boundary conditions were obtained by symmetrizing the Hamiltonian 2.68. Caution should be issued however that the above boundary conditions only apply when the Bloch functions in both well materials are similar, as is the case for the *GaAs* – *AlGaAs* system used throughout this thesis. The boundary conditions boil down to the continuity of the wave function and “generalized” continuity of its derivative, corresponding to current across the interface. The numerical implementation details of the two bands model is given in Appendix [put here the appendix of the 2 bands model](#).

As an illustration, we present in Fig. 2.7(a) the valence subband structure of a 100 *GaAs*/*Al*_{0.3}*Ga*_{0.7}*As* quantum well. The light and heavy holes are very heavily coupled, giving rise to highly non-parabolic subbands.

Particularly important is the *density of states* (DOS), which can be found from

$$\rho(E) = \frac{1}{\pi} \frac{dk}{dE}, \quad (2.84)$$

assuming the dispersion relationship is isotropic (using the axial approximation, see Appendix [put here the appendix of the 2 bands model](#)). As an illustration, we plot in Fig. 2.7(b) the calculated ratio between the DOS of the valence subbands from 2.7(a) and the DOS of the first conduction subband. The spikes in the DOS are due to the band extrema away from the zone center.

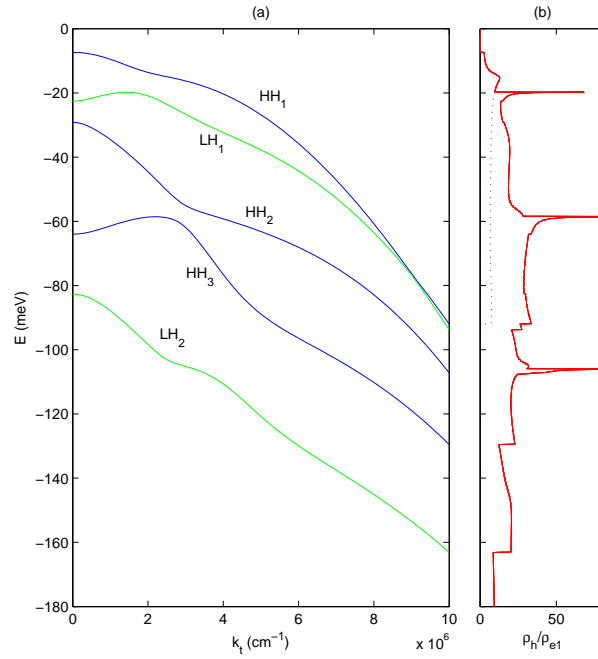


Figure 2.7: (a) Valence subbands dispersion relations calculated for a 100 wide $GaAs/Al_{0.3}Ga_{0.7}As$ quantum well, for $[100]$ crystal plane. The subbands are named after their dominant character at the zone center ($k_t = 0$). (b) The ratio between the density of states of the valence subbands and the first conduction subband, calculated for the same structure.

Chapter 3

Free Carriers Optical Transitions

Absorption and emission of photons in semiconductors and semiconductor nanostructures is the result of the complex interaction between light and condensed matter, i.e. photons, electrons, and ions. In order to capture the physics behind these processes, electromagnetism and quantum mechanics have to be combined, leading to a multitude of physical phenomena. This thesis focuses on the static properties of nanostructures, such as the constant emission or absorption of light. Therefore, the theory will be treated within the time-independent limit. The theory here is formulated within the classical limit of optical transitions, where the quantum-mechanically treated carriers couple to a classical electromagnetic field. The resulting equations are famous and denoted as *semiconductor-Bloch equations* (**author?**) [25]. These equations have been used successfully over decades to describe optical properties within semiconductors. A fully consistent treatment of the light-emission would in principle require to work in a fully quantized picture (see the review (**author?**) [30]), leading to the *semiconductor-luminescence equations*. Such a treatment is beyond the scope of this thesis. The derivation presented here serves to illustrate the imposed approximations and to clearly document the implemented equations for nanostructures of any dimensionality using the electronic structure obtained via the $\mathbf{k} \cdot \mathbf{p}$ envelope equations. This theory review is based mainly on (**author?**) [15, 27, 14, 26?].

The chapter is organized as follows. The first section covers the transfor-

3.1. SECOND QUANTIZATION OF FREE CARRIERS OPTICAL TRANSITIONS

mation of the crystal Hamiltonian 2.8 into the second quantization. Then, the representation will be rewritten in terms of the Bloch states, with a particular focus on the details arising when electronic states obtained using the $\mathbf{k} \cdot \mathbf{p}$ envelope function method are used. In the present chapter, the Coulomb interaction will be excluded and thereby, only transitions between free carriers will be considered. Coulomb-correlated transitions will be treated in Chapter [next chapter](#) .

The second section introduces the classical (monochromatic) light field and the self-consistent coupling to the electrons within the semiconductor nanostructure. The resulting equations allow to calculate the optical susceptibility and therefrom absorption, stimulated emission and refractive index change. The third section briefly explains how spontaneous emission can be obtained from optical susceptibility. The fourth section covers the procedure to calculate required matrix elements from wavefunctions obtained using the $\mathbf{k} \cdot \mathbf{p}$ envelope equations.

3.1 Second Quantization

3.1.1 Introduction

The electrons are fermions and consequently their wavefunction must be antisymmetric to obey the Pauli exclusion principle. But instead of using a complicated expression for the antisymmetric wavefunction, restricted to a constant number of particles, the Hamiltonian can be formulated in the second quantization that allows to include a varying number of particles and maintain the antisymmetry of the wavefunction naturally. Starting with the Hamiltonian 2.8 and separating the interaction with the external electromag-

3.1. SECOND QUANTIZATION FREE CARRIERS OPTICAL TRANSITIONS

netic field leads to

$$\begin{aligned}
 H = & \sum_i \underbrace{\left(\frac{\mathbf{p}_i^2}{2m_0} + U(\mathbf{r}_i) \right)}_{H_1} + \underbrace{\sum_i \left(\frac{e}{m_0} \mathbf{A}_i \cdot \mathbf{p}_i + \frac{e^2}{2m_0} \mathbf{A}_i^2 \right)}_{H_{e-EM}} \\
 & + \underbrace{\frac{1}{2} \sum_{i,j} \frac{e^2}{4\pi\epsilon_0 |\mathbf{r}_i - \mathbf{r}_j|}}_{H_2}. \tag{3.1}
 \end{aligned}$$

Here the pure electro-magnetic Hamiltonian H_{EM} has been dropped as it constitutes within the present theory only an additional energy. Let φ_n be the eigenstates of the single particle Hamiltonian H_1

$$H_1 \varphi_n = E \varphi_n \tag{3.2}$$

with resulting energies and wavefunctions. Next, the vacuum ground state $|0\rangle$ and creation and annihilation operators \hat{a}_n^\dagger and \hat{a}_n are introduced. These operators create and destroy a particle with φ_n and therefore act on the state

$$\hat{a}_n^\dagger |0\rangle = |1_n\rangle, \quad \hat{a}_n |1_n\rangle = |0\rangle, \quad \hat{a}_n |0\rangle = 0, \quad \hat{a}_n^\dagger |1_n\rangle = 0. \tag{3.3}$$

The state span an Hilbert space of varying number of particles termed as the *Fock space*. The Fock space \mathcal{F} can be defined in terms of the direct sum of N -particle Hilbert spaces \mathcal{H}_N

$$\mathcal{F} = \mathcal{H}_0 + \mathcal{H}_1 + \mathcal{H}_2 + \dots$$

The antisymmetry of the state is preserved by the fermion commutation rule

$$[\hat{a}_n^\dagger, \hat{a}_{n'}]_+ = \hat{a}_n^\dagger \hat{a}_{n'} + \hat{a}_{n'} \hat{a}_n^\dagger = \delta_{nn'} \tag{3.4}$$

and

$$[\hat{a}_n, \hat{a}_{n'}]_+ = [\hat{a}_n^\dagger, \hat{a}_{n'}^\dagger]_+ = 0. \tag{3.5}$$

3.1. ~~SECOND QUANTIZATION~~ FREE CARRIERS OPTICAL TRANSITIONS

A valuable tool to transfer the Hamiltonian 3.1 (or any other operator) into second quantization representation is given by the electron field operator

$$\hat{\Phi}(\mathbf{r}, t) = \sum_n \varphi_n(\mathbf{r}) \hat{a}_n(t). \quad (3.6)$$

Here, we switch from the Schrödinger to the Heisenberg picture. For an operator A in the Schrödinger picture, the corresponding operator in the Heisenberg picture is given by

$$A_H = e^{iHt/\hbar} A e^{-iHt/\hbar}, \quad (3.7)$$

where H is the Hamilton operator. As the Heisenberg picture will be generally used, the time-dependence of the operators is dropped from now on.

3.1.1.1 Single Particle Hamiltonian

Using the field operator $\hat{\Phi}(\mathbf{r})$, the representation of the single-particle Hamiltonian H_1 in second quantization is given by

$$\begin{aligned} \hat{H}_1 &= \int d\mathbf{r} \hat{\Phi}^\dagger(\mathbf{r}) H_1 \hat{\Phi}(\mathbf{r}) \\ &= \sum_{j,k} \hat{a}_j^\dagger \hat{a}_k \int d\mathbf{r} \varphi_j^* H_1 \varphi_k \\ &= \sum_j \hat{a}_j^\dagger \hat{a}_j E_j, \end{aligned} \quad (3.8)$$

which is diagonal as φ_n is assumed to be an eigenfunction of H_1 . The representation in terms of second quantization could also be performed using another basis of the single-particle Hilbert space, but then 3.8 would not be diagonal in jk . Another detail is that here, the first quasi-particle, a particle occupying the eigenstates of the single particle Hamiltonian H_1 , has been introduced.

3.1. SECOND QUANTIZATION OF FREE CARRIERS OPTICAL TRANSITIONS

3.1.1.2 Two Particle Hamiltonian: Coulomb Interaction

The transformation of the two-particle interaction, the Coulomb term H_2 , is similar, but more complicated. The result of the expansion is

$$\hat{H}_2 = \frac{1}{2} \sum_{j,k,l,m} \langle jk | v | lm \rangle \hat{a}_j^\dagger \hat{a}_k^\dagger \hat{a}_l \hat{a}_m. \quad (3.9)$$

The matrix element $\langle jk | v | lm \rangle$ is given by

$$\langle jk | v | lm \rangle = \int d\mathbf{r} d\mathbf{r}' \varphi_j^*(\mathbf{r}) \varphi_k^*(\mathbf{r}') \frac{e^2}{4\pi\epsilon_0 |\mathbf{r} - \mathbf{r}'|} \varphi_m(\mathbf{r}) \varphi_l(\mathbf{r}'). \quad (3.10)$$

Note that the m and the l are swapped in the integral compared to the annihilation and creation operators and that in $\langle jk | v | lm \rangle$, the spin variable must be included, so

$$\langle jk | v | lm \rangle \rightarrow \delta_{s_j s_m} \delta_{s_k s_l} \langle jk | v | lm \rangle.$$

3.1.1.3 Particle – Electromagnetic Field Interaction Hamiltonian

The next Hamiltonian to quantize is the electron–EM field interaction Hamiltonian H_{e-EM} defined in 3.1. It is clear that H_{e-EM} is a one-particle Hamiltonian and therefore its representation in the second quantization is obtained by applying the field operators as in 3.8, with the difference that φ_n is diagonal in H_1 but not in H_{e-EM} . The resulting expression reads

$$\hat{H}_{e-EM} = \sum_{j,k} \left(\frac{e}{m_0} \langle j | \mathbf{A} \cdot \mathbf{p} | k \rangle + \frac{e^2}{2m_0} \langle j | \mathbf{A}^2 | k \rangle \right) \hat{a}_j^\dagger \hat{a}_k. \quad (3.11)$$

To simplify the Hamiltonian and in order to get rid of the vector potential \mathbf{A} in favor of the electric field $\mathbf{E} = -\frac{\partial}{\partial t} \mathbf{A}$ (Coulomb gauge assumed as before), the *dipole approximation* can be applied. As the crystal is a quasi-periodic structure, where the periodicity is much smaller than the photon wavelength of usual electromagnetic fields, the electric field can be assumed to be constant within the range of a lattice cell. This approximation removes the spatial dependence of \mathbf{A} and reduces the second term $\langle j | \mathbf{A}^2 | k \rangle$ to a

3.1. ~~SECOND QUANTIZATION~~ FREE CARRIERS OPTICAL TRANSITIONS

contribution diagonal in j, k , and is therefore proportional to the number of electrons and does not contribute to any interband transitions. Therefore, it can be treated as an additional energy constant and thus be neglected. The remaining term, $\frac{e}{m_0} \langle j | \mathbf{A} \cdot \mathbf{p} | k \rangle$ is more difficult to simplify and thus a simplified argument is brought here, while the full justification can be found in [?]. The first step is to relate the momentum matrix element \mathbf{p} and the dipole transition matrix element \mathbf{r} . The relation is given by

$$[\mathbf{r}, H_1] = \frac{i\hbar}{m_0} \mathbf{p}, \quad (3.12)$$

where H_1 is the single particle Hamiltonian. Thus, the second term in 3.11 can be transformed into

$$\begin{aligned} \frac{e}{m_0} \langle j | \mathbf{A} \cdot \mathbf{p} | k \rangle &= \mathbf{A} \cdot \frac{e}{i\hbar} \langle j | [\mathbf{r}, H_1(\mathbf{r})] | k \rangle \\ &= \mathbf{A} \cdot \frac{e}{i\hbar} \langle j | \mathbf{r} H_1(\mathbf{r}) - H_1(\mathbf{r}) \mathbf{r} | k \rangle \\ &= \mathbf{A} \cdot \frac{e}{i\hbar} \langle j | \mathbf{r} | k \rangle (E_k - E_j) \\ &= -\frac{i}{\hbar} (E_k - E_j) \mathbf{A} \cdot \langle j | \mathbf{d} | k \rangle, \end{aligned} \quad (3.13)$$

where $\mathbf{d} = -e\mathbf{r}$ is the dipole moment. The last step involved adding the term $\mathbf{d}_{j,k} \cdot \mathbf{E} - \mathbf{d}_{j,k} \cdot \mathbf{E}$, which with the definition of \mathbf{E} gives

$$\frac{e}{m_0} \langle j | \mathbf{A} \cdot \mathbf{p} | k \rangle = -\mathbf{d}_{j,k} \cdot \mathbf{E} - \left(\frac{\hbar}{i} \frac{\partial}{\partial t} + E_j - E_k \right) \mathbf{A} \cdot \mathbf{d}_{j,k}. \quad (3.14)$$

If \mathbf{A} is given by a plane wave $\mathbf{A}_0 e^{i(\omega_0 t - \mathbf{k}_0 \cdot \mathbf{r})}$ with center frequency ω_0 and the transition energies $E_k - E_j$ are ranged around $\hbar\omega_0$, the expression in the brackets vanished and the dipole approximation for the Hamiltonian is obtained,

$$\hat{H}_{e-EM} = - \sum_{j,k} \langle j | \mathbf{d} \cdot \mathbf{E} | k \rangle \hat{a}_j^\dagger \hat{a}_k. \quad (3.15)$$

The final Hamiltonian for the crystal electrons 3.1, can therefore be

3.1. SECOND QUANTIZATION FREE CARRIERS OPTICAL TRANSITIONS

written as

$$\hat{H} = \sum_{j,k} \langle j | H_1 | k \rangle \hat{a}_j^\dagger \hat{a}_k + \frac{1}{2} \sum_{j,k,l,m} \langle jk | v | lm \rangle \hat{a}_j^\dagger \hat{a}_k^\dagger \hat{a}_l \hat{a}_m - \sum_{j,k} \langle j | \mathbf{d} \cdot \mathbf{E} | k \rangle \hat{a}_j^\dagger \hat{a}_k. \quad (3.16)$$

3.1.2 Bloch States Formulation

Up to now, we have ignored the specific form of the wavefunction φ_n . Here we consider the wavefunction to be a Bloch function, as presented in Chapter [the electronic states structure](#). Within a bulk crystal, the Bloch function is given by

$$\varphi_{n\mathbf{k}}(\mathbf{r}) = u_{n\mathbf{k}}(\mathbf{r}) e^{i\mathbf{k} \cdot \mathbf{r}}, \quad (3.17)$$

where $u_{n\mathbf{k}}(\mathbf{r})$ is lattice periodic and the exponential term is slowly varying. The current section aims now to transform 3.16 into Bloch states, which needs some clarifications and definitions.

The Bloch-functions are required to be orthonormalized over the crystal domain Ω

$$\int_{\Omega} d\mathbf{r} \varphi_{n'\mathbf{k}'}^* \varphi_{n\mathbf{k}} = \delta_{n',n} \delta_{\mathbf{k}',\mathbf{k}}. \quad (3.18)$$

The goal now is to represent the Hamiltonian 3.16 using the field operator

$$\hat{\Phi}(\mathbf{r}, t) = \sum_{n,\mathbf{k}} \varphi_{n\mathbf{k}} \hat{a}_{n\mathbf{k}}(t) \quad (3.19)$$

in terms of the Bloch-functions. As the Bloch-states are not localized, the Fourier transform of certain quantities (such as the electromagnetic field or the Coulomb interaction) in the translational invariant directions will be used to simplify the Hamiltonian. For the spatial Fourier transform, the conventions are given by

$$w(\mathbf{r}) = \sum_{\mathbf{q}} w(\mathbf{q}) e^{i\mathbf{q} \cdot \mathbf{r}}, \quad (3.20)$$

$$w(\mathbf{q}) = \frac{1}{\mathcal{A}} \int_{\mathcal{A}} d\mathbf{r} w(\mathbf{r}) e^{-i\mathbf{q} \cdot \mathbf{r}}. \quad (3.21)$$

3.1. ~~SECOND QUANTIZATION~~ ~~FREE~~ CARRIERS OPTICAL TRANSITIONS

3.1.2.1 Normalization

In the case of a quantum nanostructure, the Bloch function loses its plane wave dependence in the quantized direction and is therefore expressed as

$$\varphi_{n\mathbf{k}}(\mathbf{r}, z) = |n\mathbf{k}\rangle = u_{n\mathbf{k}}(\mathbf{r}, z)e^{i\mathbf{k}\cdot\mathbf{r}}F_{n\mathbf{k}}(z). \quad (3.22)$$

The free direction is represented by the plane-wave and the symmetry broken part by $F(z)$. The indices n now include the subbands. In the following, the coordinate z will be used for the symmetry broken direction while \mathbf{r} will denote the translational invariant direction.

Regarding the normalization, it is assumed that \mathcal{A} is the volume of the translational invariant direction and \mathcal{L} is the volume of the quantized direction. Obviously, $\Omega = \mathcal{L}\mathcal{A}$. 3.18 is still required to hold, but the normalization over the translational invariant direction is distributed into the lattice periodic part $u_{n\mathbf{k}}(\mathbf{r}, z)$. The envelope function $F(z)$ is then normalized over the quantized direction. Therefore, for a system quantized in d dimensions, the units of the wavefunction parts are given by

$$\underbrace{\varphi_{n\mathbf{k}}(\mathbf{r}, z)}_{\frac{1}{\sqrt{m^3}} = \frac{1}{\sqrt{\Omega}}} = \underbrace{u_{n\mathbf{k}}(\mathbf{r}, z)}_{\frac{1}{\sqrt{m^{3-d}}} = \frac{1}{\sqrt{\mathcal{A}}}} e^{i\mathbf{k}\cdot\mathbf{r}} \underbrace{F_{n\mathbf{k}}(z)}_{\frac{1}{\sqrt{m^d}} = \frac{1}{\sqrt{\mathcal{L}}}}. \quad (3.23)$$

3.1.2.2 Lattice-Cell Average

A general problem of the approach using wavefunctions of the $\mathbf{k} \cdot \mathbf{p}$ envelope equation is that the lattice-periodic functions $u_{n\mathbf{k}}(\mathbf{r}, z)$ are not given in an explicit form. Only their symmetry properties, the fact that they are orthogonal to each other and some measurable quantities are available. Nevertheless, these properties are sufficient for building the Hamiltonian and calculating desired matrix elements, within the approximation that lattice-cell averaged quantities are used. In the $\mathbf{k} \cdot \mathbf{p}$ method, the envelopes and plane waves are assumed to vary little over a crystal cell. If an operator A mainly acts on the lattice-periodic part, a matrix element between two wavefunctions 3.22

3.1. ~~SECOND QUANTIZATION~~ FREE CARRIERS OPTICAL TRANSITIONS

can be simplified as

$$\langle n' \mathbf{k}' | A | n \mathbf{k} \rangle \approx \frac{\mathcal{A}}{V_c} \langle u_{n' \mathbf{k}'} | A | u_{n \mathbf{k}} \rangle_{V_c} \delta_{k', k} \int dz F_{n' \mathbf{k}'}^*(z) F_{n \mathbf{k}}(z). \quad (3.24)$$

Here the operator A is replaced with it's lattice averaged quantity

$$V_c^{-1} \langle u_{n' \mathbf{k}'} | A | u_{n \mathbf{k}} \rangle_{V_c}.$$

V_c denotes the crystal cell and $\langle \rangle_{V_c}$ the integration over it. The matrix elements found in the literature are related by

$$\frac{\mathcal{A}}{V_c} \langle u_{n' \mathbf{k}'} | A | u_{n \mathbf{k}} \rangle_{V_c} = \langle \tilde{u}_{n' \mathbf{k}'} | A | \tilde{u}_{n \mathbf{k}} \rangle \quad (3.25)$$

where \tilde{u}_i is the Bloch function normalized with respect to a single crystal cell. Therefore to determine values for the short-range operator $\langle n' \mathbf{k}' | A | n \mathbf{k} \rangle$, only the envelope function $F_{n \mathbf{k}}(z)$ and the experimental value for $\langle \tilde{u}_{n' \mathbf{k}'} | A | \tilde{u}_{n \mathbf{k}} \rangle$ for the from bulk measurements are required.

The other case is given by the long-range operator B , such as the Coulomb potential. In that case, the operator is constant over a lattice cell and the integral of the matrix element can be reduced using the orthogonality of the Bloch functions. The lattice-cell average reads

$$\begin{aligned} \langle n' \mathbf{k}' | B | n \mathbf{k} \rangle &= \int_{\Omega} d\mathbf{r} dz u_{n' \mathbf{k}'}^*(\mathbf{r}, z) e^{-i\mathbf{k}' \cdot \mathbf{r}} F_{n' \mathbf{k}'}^*(z) B u_{n \mathbf{k}}(\mathbf{r}, z) e^{i\mathbf{k} \cdot \mathbf{r}} F_{n \mathbf{k}}(z) \\ &\approx \int_{\Omega} d\mathbf{r} dz \frac{1}{V_c} \langle u_{n' \mathbf{k}'} | u_{n \mathbf{k}} \rangle_{V_c} e^{-i\mathbf{k}' \cdot \mathbf{r}} F_{n' \mathbf{k}'}^*(z) B u_{n \mathbf{k}}(\mathbf{r}, z) e^{i\mathbf{k} \cdot \mathbf{r}} F_{n \mathbf{k}}(z) \end{aligned} \quad (3.26)$$

A further simplification depends on the actual form of the considered operator.

3.1.2.3 The Kinetic Term

To transform the kinetic part into the Bloch states, the eigenfunctions $\varphi_{n \mathbf{k}}(\mathbf{r}, z)$ of the single particle Hamiltonian are inserted into the field operator. Using

3.1.2.4 THE QUANTIZED FREE CARRIERS OPTICAL TRANSITIONS

that particular field operator, the kinetic term 3.16 is given by

$$\hat{H}_1 = \sum_{n,\mathbf{k}} \hat{a}_{n\mathbf{k}}^\dagger \hat{a}_{n\mathbf{k}} E_{n,\mathbf{k}}. \quad (3.27)$$

3.1.2.4 The Interaction Term

The remaining step is to quantize the electron - electromagnetic field interaction Hamiltonian H_{e-EM} within the dipole approximation. The Fourier representation of the electric field $\mathbf{E}(\mathbf{r}, t)$ is given by

$$\mathbf{E}(\mathbf{r}, t) = \sum_{\mathbf{q}} \mathbf{E}(\mathbf{q}, t) e^{i\mathbf{q}\cdot\mathbf{r}}. \quad (3.28)$$

As it is assumed that $\mathbf{E}(\mathbf{r}, t)$ is slowly-varying, the relevant contributions to the sum will be around very small values of \mathbf{q} . This allows to pull the $e^{i\mathbf{q}\cdot\mathbf{r}}$ factor out of the dipole integral in the calculation below. The resulting Hamiltonian then reads

$$\begin{aligned} & \int_{\Omega} d\mathbf{r} dz \hat{\Phi}^\dagger H_{e-EM} \hat{\Phi} \\ &= - \sum_{n',\mathbf{k}',n,\mathbf{k}} \hat{a}_{n'\mathbf{k}'}^\dagger \hat{a}_{n\mathbf{k}} \int_{\Omega} d\mathbf{r} dz \varphi_{n'\mathbf{k}'}^* \mathbf{d} \cdot \left(\sum_{\mathbf{q}} \mathbf{E}(\mathbf{q}, t) e^{i\mathbf{q}\cdot\mathbf{r}} \right) \varphi_{n\mathbf{k}} \\ &= - \sum_{n',\mathbf{k}',n,\mathbf{k}} \sum_{\mathbf{q}} \delta_{\mathbf{k}'\mathbf{k}} \boldsymbol{\mu}_{n',n,\mathbf{k}} \cdot \mathbf{E}(\mathbf{r}, t) e^{i\mathbf{q}\cdot\mathbf{r}}, \end{aligned}$$

where the dipole matrix element between two states n and n' with same crystal momentum \mathbf{k} is given by

$$\boldsymbol{\mu}_{n',n,\mathbf{k}} = \mathcal{A} \int_{\mathcal{L}} dz u_{n'\mathbf{k}}^* F_{n'\mathbf{k}}^* \mathbf{d} u_{n\mathbf{k}} F_{n\mathbf{k}}. \quad (3.29)$$

The delta function $\delta_{\mathbf{k}'\mathbf{k}}$ results from the plane wave and ensures momentum conservation. In other words, only direct transitions are allowed. Using the dipole matrix element, the Hamiltonian can finally be written as

$$\hat{H}_{e-EM} = -\mathbf{E}(\mathbf{r}, t) \sum_{n',n,\mathbf{k}} \boldsymbol{\mu}_{n',n,\mathbf{k}} \hat{a}_{n'\mathbf{k}}^\dagger \hat{a}_{n\mathbf{k}}. \quad (3.30)$$

3.1. SECOND QUANTIZATION OF FREE CARRIERS OPTICAL TRANSITIONS

The transformation of the two particle Hamiltonian H_2 is presented in the next chapter. For the moment, it is assumed that the carriers are *uncorrelated* and their coulomb interaction is included in the single particle Hamiltonians. Collecting all single particle interactions, the Hamiltonian in the Bloch basis is given as

$$\hat{H} = \sum_n E_n(\mathbf{k}) \hat{a}_{n\mathbf{k}}^\dagger \hat{a}_{n\mathbf{k}} - \mathbf{E}(\mathbf{r}, t) \sum_{n', n, \mathbf{k}} \boldsymbol{\mu}_{n', n, \mathbf{k}} \hat{a}_{n'\mathbf{k}}^\dagger \hat{a}_{n\mathbf{k}}. \quad (3.31)$$

3.1.3 Holes

In a semiconductor at $T = 0K$, the valence band is fully occupied while the conduction band is empty. With increasing temperature, electrons in the valence band get excited into the conduction band and leave behind holes. Consequently, it is common to use for the valence band the absence of an electron, the hole, as a quasi particle. Therefore, if an electron with momentum $-\mathbf{k}$ is created ($= \hat{a}_{-\mathbf{k}}^\dagger$), a hole with momentum \mathbf{k} is annihilated ($= \hat{b}_{\mathbf{k}}$) and vice versa. The sign is switched by convention. In order to introduce the concept of holes into the Hamiltonian, the commutator rules 3.4 and 3.5 are used to reestablish the normal ordering of creation and annihilation operators. One obtains for the kinetic and dipole Hamiltonian

$$\begin{aligned} \hat{H} = & \sum_{c, \mathbf{k}} E_c(\mathbf{k}) \hat{a}_{c\mathbf{k}}^\dagger \hat{a}_{c\mathbf{k}} - \sum_{v, \mathbf{k}} E_v(\mathbf{k}) \hat{b}_{v\mathbf{k}}^\dagger \hat{b}_{v\mathbf{k}} \\ & - \mathbf{E}(\mathbf{r}, t) \left(\sum_{c, v, \mathbf{k}} \boldsymbol{\mu}_{cv, \mathbf{k}} \underbrace{\hat{a}_{c\mathbf{k}}^\dagger \hat{b}_{v-\mathbf{k}}^\dagger}_{\hat{p}_{vc, \mathbf{k}}^\dagger} + \boldsymbol{\mu}_{cv, \mathbf{k}}^* \underbrace{\hat{b}_{v-\mathbf{k}} \hat{a}_{c\mathbf{k}}}_{\hat{p}_{vc, \mathbf{k}}} \right). \end{aligned} \quad (3.32)$$

Note that from now on, the summation is distinguished between summation over conduction bands indicated with c and valence bands indicated using the index v . In 3.32, transitions between conduction subbands and transitions between valence subbands have been neglected.

One important point is that in the Hamiltonian 3.32, some terms can already be identified: $\hat{n}_{c\mathbf{k}} = \hat{a}_{c\mathbf{k}}^\dagger \hat{a}_{c\mathbf{k}}$ is the number operator counting the

3.1. ~~SECOND QUANTIZATION~~ FREE CARRIERS OPTICAL TRANSITIONS

number of electrons in the band c with crystal momentum \mathbf{k} , while $\hat{n}_{vk} = \hat{b}_{b-\mathbf{k}}^\dagger \hat{b}_{b-\mathbf{k}}$ is the number operator counting the holes in the valence band v . The term $\hat{p}_{vc,\mathbf{k}} = \hat{b}_{v-\mathbf{k}} \hat{a}_{c\mathbf{k}}$ is named *microscopic polarization* and is given by the off-diagonal density matrix element, giving the correlation between a particle in one band and an empty state in the other. In a simplistic view, the dipole matrix element $\boldsymbol{\mu}_{cv,\mathbf{k}}$ gives the coupling strength of such a correlation to an electric field.

3.1.4 Carrier Statistics

The main interest of the current work is the continuous emission of light of a semiconductor, which is given in the steady state of the system. In the limit of small light intensity and therefore absence of spectral-hole burning, it can be assumed that the carriers relax into their quasi-equilibrium distributions, given by the Fermi distributions for the electrons in the conduction band

$$n_{c\mathbf{k}} = \langle \hat{n}_{c\mathbf{k}} \rangle = f_{c\mathbf{k}} = \frac{1}{1 + e^{(E_c(\mathbf{k}) - E_{F,c})/k_B T}} \quad (3.33)$$

and the holes in the valence band

$$n_{v\mathbf{k}} = \langle \hat{n}_{v\mathbf{k}} \rangle = f_{v\mathbf{k}} = \frac{1}{1 + e^{(E_{F,v} - E_v(\mathbf{k}))/k_B T}}. \quad (3.34)$$

Here, $E_{F,c}$ and $E_{F,v}$ denote the quasi-Fermi levels of the electrons and holes, k_B is Boltzmann's constant and T denotes the temperature. The Fermi levels can be calculated from the 3D carrier density N

$$N = \frac{1}{\Omega} \sum_{c\mathbf{k}} f_{c\mathbf{k}} \quad (3.35)$$

for electrons and P

$$P = \frac{1}{\Omega} \sum_{v\mathbf{k}} f_{v\mathbf{k}} \quad (3.36)$$

3.2. TRANSITION PROBABILITIES FOR GENERAL BAND STRUCTURES

for holes. Here Ω denotes the volume of the system, which is usually unknown. When the sum over \mathbf{k} is transformed into an integral

$$\sum_{\mathbf{k}} \rightarrow \frac{\mathcal{A}}{(2\pi)^d} \int d\mathbf{k} \quad (3.37)$$

the unknown Ω volume is removed and one ends up with known quantities ($\mathcal{L} = \Omega/\mathcal{A}$). d denotes the dimensionality of the \mathbf{k} -space. As the \mathbf{k} dependence of the distributions for general band structures is quite evolved, an analytical inversion of 3.35 and 3.36 is not feasible. Therefore, the simplest way to calculate the quasi-Fermi levels is to perform a numerical Newton procedure to find the roots of $N_0 - N(E_F) = 0$.

3.2 Transitions Calculation

3.2.1 Introduction

Classically, an electric field \mathbf{E} in a semiconductor induces dipoles. These dipoles create a macroscopic polarization \mathbf{P} . The induced polarization $\mathbf{P}(t)$ at time t depends on the electric field $\mathbf{E}(t')$ at time $t' < t$. Their relation is defined in terms of a time-dependent susceptibility $\chi(t - t')$ (in this case a scalar)

$$\mathbf{P}(t) = \epsilon_b \int_{-\infty}^t \chi(t - t') \mathbf{E}(t') dt'. \quad (3.38)$$

Taking the Fourier transform of 3.38 leads to the more convenient form

$$\mathbf{P}(\omega) = \epsilon_b \chi(\omega) \mathbf{E}(\omega). \quad (3.39)$$

The polarization influences the electric field via the electric displacement

$$\mathbf{D} = \epsilon \mathbf{E} = \epsilon_b \mathbf{E} + \mathbf{P}. \quad (3.40)$$

Therefore, the creation of dipoles and the amplification of an electric field needs to be treated self-consistently. The aim is therefore to calculate the polarization quantum-mechanically in the presence of an electric field and

3.2. TRANSFERAL CARRIER OPTICAL TRANSITIONS

obtain a self-consistent formula for the steady state.

As a first step, Maxwell's equations are rewritten to give a single relation between the electric field \mathbf{E} and the macroscopic polarization \mathbf{P} . Taking the curl of

$$\nabla \times \mathbf{H} - \frac{\partial \mathbf{D}}{\partial t} = \mathbf{j} \quad (3.41)$$

and using

$$\nabla \times \mathbf{E} = -\frac{\partial \mathbf{B}}{\partial t}, \quad (3.42)$$

ones obtains

$$\nabla \times \nabla \times \mathbf{E} = -\nabla \times \frac{\partial \mu_0 \mathbf{H}}{\partial t}, \quad (3.43)$$

$$\nabla (\nabla \cdot \mathbf{E}) - \nabla^2 \mathbf{E} = -\mu_0 \frac{\partial}{\partial t} (\nabla \times \mathbf{H}). \quad (3.44)$$

On the left hand side, the term $\nabla \cdot \mathbf{E} = 0$ vanishes, assuming charge neutrality and homogeneous media. On the right hand side, using 3.41, $\nabla \times \mathbf{H}$ is replaced by the electric displacement \mathbf{D}

$$\nabla (\nabla \cdot \mathbf{E}) - \nabla^2 \mathbf{E} \approx -\nabla^2 \mathbf{E} = -\mu_0 \frac{\partial^2 \mathbf{D}}{\partial t^2}, \quad (3.45)$$

which now allows to introduce the macroscopic polarization \mathbf{P} using 3.40

$$-\nabla^2 \mathbf{E} + \mu_0 \epsilon_b \frac{\partial^2 \mathbf{E}}{\partial t^2} = -\mu_0 \frac{\partial^2 \mathbf{P}}{\partial t^2}. \quad (3.46)$$

This equation is the *inhomogeneous Helmholtz equation*. The next step is to assume a monochromatic electrical field \mathbf{E} (traveling into z -direction) given by

$$\mathbf{E}(z, t) = \frac{1}{2} \hat{e}_i E(z) e^{i(k_0 z - \nu t - \phi(z))} + \text{c.c.}, \quad (3.47)$$

where $k_0 = \nu n/c$ is the photo wavenumber and \hat{e}_i is a unit vector orthogonal to \hat{e}_z . $\phi(z)$ is the real phase shift and $E(z)$ is the real field amplitude, varying little within an optical wavelength. ν denotes the field frequency. It is assumed that the spacial strong oscillatory part is properly described by

3.2. TRANSFER OF ENERGY FROM CARRIER OPTICAL TRANSITIONS

the plane wave. The electric field induces a polarization

$$\mathbf{P}(z, t) = \frac{1}{2} \hat{\mathbf{e}}_i P(z) e^{i(k_0 z - \nu t - \phi(z))} + \text{c.c.} \quad (3.48)$$

The next step is to insert 3.47 and 3.48 into 3.46 and neglect all terms containing $\partial_z^2 E(z)$, $\partial_z^2 \phi(z)$ and $\partial_z E(z) \partial_z \phi(z)$. This approach is denoted as the *slowly varying envelope approximation* and one ends up with an equation for the amplitudes $E(z)$ and $P(z)$,

$$\partial_z E(z) - iE(z) \partial_z \phi(z) = i \frac{\mu_0 \nu^2}{2k_0} \chi(z) E(z). \quad (3.49)$$

Splitting into real and imaginary parts and using 3.39, the *self consistent* equations are obtained as

$$\partial_z E(z) = -\frac{\nu}{2\epsilon_0 n c} \Im \{P(z)\} = -\frac{k_0}{2} \chi''(z) E(z) \quad (3.50)$$

$$\partial_z \phi(z) = -\frac{1}{E(z)} \frac{\nu}{2\epsilon_0 n c} \Re \{P(z)\} = -\frac{k_0}{2} \chi'(z) \quad (3.51)$$

where $\chi = \chi' + i\chi''$. Consequently, the intensity gain (amplitude is half of it) is defined by

$$G = -k_0 \chi'' \quad (3.52)$$

and the change of refractive index (via a continuous phase change) is given by the real part of the susceptibility

$$\frac{\delta n}{n} = \frac{\chi'}{2}. \quad (3.53)$$

3.2.2 Quantum Microscopic Polarization

The second step is to couple quantum mechanical observables to the solids properties. The dipole interaction between electrons and the electric field is given by

$$H_{e-EM} = -V \mathbf{P} \cdot \mathbf{E}, \quad (3.54)$$

3.2. TRANSFER OF ENERGY FROM CARRIER TO PHOTON

where V is the volume of the system and \mathbf{P} is defined as the macroscopic polarization density

$$\mathbf{P} = \frac{1}{V} \sum_{n,n',\mathbf{k}} \boldsymbol{\mu}_{n'n,\mathbf{k}} \langle \hat{a}_{n'\mathbf{k}}^\dagger \hat{a}_{n\mathbf{k}} \rangle = \frac{1}{V} \sum_{c,v,\mathbf{k}} \boldsymbol{\mu}_{cv,\mathbf{k}} p_{vc,\mathbf{k}}^\dagger + \boldsymbol{\mu}_{cv,\mathbf{k}}^* p_{vc,\mathbf{k}} \quad (3.55)$$

from which the optical properties 3.52 and 3.53 can be obtained. Here, the expectation value $p_{vc,\mathbf{k}} = \langle \hat{p}_{vc,\mathbf{k}} \rangle$ has been used. The amplitude $P(z)$ of the macroscopic polarization $\mathbf{P}(z, t)$ used for the optical properties is given by

$$P(z) = 2e^{-i(k_0 z - \nu t - \phi(z))} \frac{1}{V} \sum_{c,v,\mathbf{k}} \boldsymbol{\mu}_{cv,\mathbf{k}}^* p_{vc,\mathbf{k}} \quad (3.56)$$

The other term of the polarization containing $p_{vc,\mathbf{k}}^\dagger$ is related to the complex conjugate part of 3.48 and is not required to determine the macroscopic amplitude $P(z)$.

3.2.3 Heisenberg's Equation of Motion

In order to calculate the expectation value $p_{nm,\mathbf{k}}$, the equation of motion of the microscopic polarization operator $\hat{p}_{nm,\mathbf{k}}$ has to be solved. Here the index m is used for the conduction band and n for the valence band of interest. The indices c and v will be used for the summation over remaining conduction and valence bands. The Heisenberg equation of motion for a time dependent operator \hat{O} is given by

$$\frac{d}{dt} \hat{O} = \frac{i}{\hbar} [\hat{H}, \hat{O}]. \quad (3.57)$$

Applying to the microscopic polarization operator, one obtains

$$\frac{d}{dt} \hat{p}_{nm,\mathbf{k}} = \frac{i}{\hbar} [\hat{H}_1, \hat{p}_{nm,\mathbf{k}}] + \frac{i}{\hbar} [\hat{H}_{e-EM}, \hat{p}_{nm,\mathbf{k}}]. \quad (3.58)$$

The evaluation of the first commutator gives

$$- \frac{i}{\hbar} (E_c(\mathbf{k}) - E_v(\mathbf{k})) \hat{p}_{nm,\mathbf{k}}. \quad (3.59)$$

3.2. TRANSITION PROBABILITIES FOR OPTICAL TRANSITIONS

For the second operator

$$\frac{1}{V} \sum_{c,v,\mathbf{k}'} \boldsymbol{\mu}_{cv,\mathbf{k}'} \hat{p}_{vc,\mathbf{k}'}^\dagger + \boldsymbol{\mu}_{cv,\mathbf{k}'}^* \hat{p}_{vc,\mathbf{k}'}, \quad (3.60)$$

the second term containing $\hat{p}_{vc,\mathbf{k}}$ vanishes because four anticommuting exchanges are required (leading to no sign change) to obtain $\hat{p}_{nm,\mathbf{k}} \hat{H} - \hat{H} \hat{p}_{nm,\mathbf{k}} = 0$. Therefore, one is left with the first term, where operators are exchanged to transform $\hat{H} \hat{p}$ into $\hat{p} \hat{H}$

$$\begin{aligned} \hat{a}_{c\mathbf{k}'}^\dagger \hat{b}_{c-\mathbf{k}'}^\dagger \hat{b}_{n\mathbf{k}} \hat{a}_{m\mathbf{k}} &\rightarrow \hat{a}_{c\mathbf{k}'}^\dagger \hat{a}_{m\mathbf{k}} \delta_{v,n} \delta_{\mathbf{k}',\mathbf{k}} \\ &+ \hat{b}_{v-\mathbf{k}'}^\dagger \hat{b}_{n-\mathbf{k}} \delta_{c,m} \delta_{\mathbf{k}',\mathbf{k}} \\ &- \delta_{\mathbf{k}',\mathbf{k}} \delta_{n,v} \delta_{m,c} + \hat{p} \hat{H}. \end{aligned} \quad (3.61)$$

The delta functions of the remaining terms lead in the sum over c, v and \mathbf{k}' to

$$\sum_c \hat{a}_{c\mathbf{k}}^\dagger \hat{a}_{m\mathbf{k}} + \sum_v \hat{b}_{v-\mathbf{k}} \hat{b}_{n-\mathbf{k}} - 1. \quad (3.62)$$

Here, the sums over c and v except for $c = m$ and $v = n$ will vanish when later the expectation value $\langle \hat{a}_{c\mathbf{k}}^\dagger \hat{a}_{m\mathbf{k}} \rangle$ is taken. Therefore, the sums are neglected from now on. This approximation scheme is called the *random phase approximation*. The hand waving argument is that the expectation value $\langle \hat{a}_{n'\mathbf{k}'}^\dagger \hat{a}_{n\mathbf{k}} \rangle$ has a dominant time-dependence

$$\langle \hat{a}_{n'\mathbf{k}'}^\dagger \hat{a}_{n\mathbf{k}} \rangle \propto e^{i(\omega_{n'\mathbf{k}'} - \omega_{n\mathbf{k}})t} \quad (3.63)$$

and therefore rapidly oscillates for $\omega_{n'\mathbf{k}'} \neq \omega_{n\mathbf{k}}$ and then averages out over time.

The terms with $c = m$ and $v = n$ are the density operators $\hat{n}_{m\mathbf{k}}$ and $\hat{n}_{n\mathbf{k}}$. Collecting everything and taking the expectation values, the equation

3.2. TRANSFERAL CARRIER OPTICAL TRANSITIONS

of motion of the free carrier microscopic polarization is

$$\begin{aligned} \frac{d}{dt} p_{nm,\mathbf{k}} = & -\frac{i}{\hbar} (E_m(\mathbf{k}) - E_n(\mathbf{k})) p_{nm,\mathbf{k}} \\ & -\frac{i}{\hbar} \mathbf{E}(z, t) \cdot \boldsymbol{\mu}_{mn,\mathbf{k}} (n_{m\mathbf{k}} + n_{n\mathbf{k}} - 1) \\ & + \left. \frac{\partial}{\partial t} p_{nm,\mathbf{k}} \right|_{col.} \end{aligned} \quad (3.64)$$

This equation is part of the *semiconductor Bloch equations*. The last term is added as an additional term leading to polarization decay, caused by scattering. Scattering here is a electron-phonon or electron-electron process which requires a more sophisticated treatment. For the moment, scattering is approximated using a simple decay rate model given by

$$\left. \frac{\partial}{\partial t} p_{nm,\mathbf{k}} \right|_{col.} \approx -\gamma p_{nm,\mathbf{k}}. \quad (3.65)$$

3.2.4 Solving the Free Carrier Equation

To solve 3.64 one could use the approach given in 14 and formally integrate the differential equation. A simpler way is to replace the oscillating microscopic polarization $p_{nm,\mathbf{k}}$ by its slowly varying envelope

$$s_{nm,\mathbf{k}} = p_{nm,\mathbf{k}} e^{-i(k_0 z - \nu t - \phi(z))} \quad (3.66)$$

and solve for the steady state of

$$\frac{d}{dt} s_{nm,\mathbf{k}} = 0. \quad (3.67)$$

Inserting 3.66 and 3.47 into 3.64, and skipping all fast oscillating parts (as they should average out over time), leads to

$$p_{nm,\mathbf{k}} = -\frac{i}{\hbar} \frac{E(z)}{2} \mu_{mn,\mathbf{k}} \frac{n_{m\mathbf{k}} + n_{n\mathbf{k}} - 1}{i(\omega - \nu) + \gamma} e^{-i(k_0 z - \nu t - \phi(z))}. \quad (3.68)$$

3.3. SPONTANEOUS EMISSION CARRIERS OPTICAL TRANSITIONS

Inserting this equation into 3.52 we obtain the amplification of the light field intensity

$$G = -k_0 \chi'' = \frac{\nu}{\epsilon_0 n_b c} \frac{1}{\hbar} \frac{1}{\Omega} \sum_{c,v,\mathbf{k}} |\mu_{cv,\mathbf{k}}|^2 (n_{c\mathbf{k}} + n_{v\mathbf{k}} - 1) \frac{\gamma}{(\omega - \nu)^2 + \gamma^2}. \quad (3.69)$$

Here, the $\mu_{cv,\mathbf{k}}$ denotes the dipole along the polarization of the light field, resulting from the scalar product between the monochromatic light field \mathbf{E} and the dipole $\boldsymbol{\mu}_{cv,\mathbf{k}}$.

3.3 Spontaneous Emission

The spontaneous emission within a semiconductor nanostructure can be obtained from the amplification G of the photon field, i.e. the complex part of the optical susceptibility χ'' . Using a phenomenological approach, 3.69 can be divided into an emitting and an absorbing part, $G = G_e - G_a$. The term $n_{c\mathbf{k}} + n_{v\mathbf{k}} - 1$ is the inversion of the electron-hole population in the semiconductor, which can be rewritten to

$$n_{c\mathbf{k}} + n_{v\mathbf{k}} - 1 = n_{c\mathbf{k}} n_{v\mathbf{k}} - (1 - n_{c\mathbf{k}})(1 - n_{v\mathbf{k}}). \quad (3.70)$$

The first term on rhs denotes the probability of a photon emission, i.e. electron and hole is occupied, while the second term denotes the probability of a photon absorption. Therefore by evaluating 3.69 including only the emission probability term $G_e \sim n_{c\mathbf{k}} n_{v\mathbf{k}}$, the spontaneous emission probability per unit length is obtained. As the velocity of a photon in the semiconductor is given by c/n_b , the spontaneous emission probability per second is given by $G_e c/n_b$. Neglecting the existence of a cavity, the photon density of states (of photons with energy $\hbar\omega$) is given by

$$N(\hbar\omega) = \frac{n_b^3 (\hbar\omega)^2}{\pi^2 \hbar^3 c^3} \quad (3.71)$$

3.3. SPONTANEOUS EMISSION CARRIERS OPTICAL TRANSITIONS

and therefore the spontaneous emission ($s^{-1}m^{-3}eV^{-1}$) per second per unit volume per unit energy is given by

$$r_{sp}(\hbar\omega) = \frac{n_b^3(\hbar\omega)^2}{\pi^2\hbar^3c^2}G_e \quad (3.72)$$

where as the spontaneous emission intensity ($s^{-1}m^{-3}$) is given by

$$I_{sp}(\hbar\omega) = \hbar\omega r_{sp}(\hbar\omega). \quad (3.73)$$

Note that the result can be related to the Kubo-Martin-Schwinger (KMS) relation. The relation between emission and inversion gives

$$\frac{f_{c\mathbf{k}}f_{v\mathbf{k}}}{f_{c\mathbf{k}} + f_{v\mathbf{k}} - 1} = \frac{1}{1 - \exp((E_c(\mathbf{k}) - E_v(\mathbf{k}) - (E_{Fc} - E_{Fv}))/k_B T)}. \quad (3.74)$$

Due to the Lorentzian in 3.69, the transition energy $E_c(\mathbf{k}) - E_v(\mathbf{k})$ is close to the photon energy. Consequently, it may be replaced with $\hbar\omega$ on the r.h.s of 3.74, which allows to pull the factor 3.74 out of the k -sum in 3.69, leading to the KMS relation

$$r_{sp}(\hbar\omega) = \frac{n_b^2(\hbar\omega)^2}{\pi^2\hbar^3c^2} \frac{1}{1 - \exp((\hbar\omega - (E_{Fc} - E_{Fv}))/k_B T)} G(\hbar\omega) \quad (3.75)$$

between gain and spontaneous emission.

Another aspect to consider is the dependence of the dipole matrix element $\mu_{cv,\mathbf{k}}$ on the polarization of the light field. Therefore, the average of all possible transitions is usually taken for the spontaneous emission

$$\mu_{cv,\mathbf{k}}^{sp} = \frac{1}{3} \sum_{i=x,y,z} \mu_{cv,\mathbf{k}}^i. \quad (3.76)$$

The spontaneous emission rate per unit volume ($s^{-1}m^{-3}$) is given by integrating $r_{sp}(\hbar\omega)$ over the energy

$$R_{sp} = \int_0^\infty r_{sp}(\hbar\omega) d\hbar\omega = Bnp \quad (3.77)$$

which defines another figure of merit, the spontaneous emission B coefficient ($m^3 s^{-1}$).

There is an obvious pathological feature when such a relation is used to obtain the spontaneous emission: if the electric field is zero, then no spontaneous emission would exist. The root of this misbehavior is due to the fact that the quantization of the electro-magnetic field is not included. Including this, spontaneous emission would occur - spontaneously. Nevertheless, the spontaneous emission of a two level system treated using quantized electro-magnetic fields does not differ from dipole radiation, therefore the error of the classical treatment may be small enough for the present purpose.

3.4 Dipole Matrix Element

The evaluation of the interband dipole matrix element $\mu_{mn,\mathbf{k}}$ between the solutions of the $\mathbf{k} \cdot \mathbf{p}$ band structure calculation is not straight-forward. In the general case, the envelope functions are given by

$$\varphi_{m\mathbf{k}} = \sum_i F_{m,i\mathbf{k}} u_{i0}, \quad (3.78)$$

where u_{i0} are again zone-center Bloch functions. Using this expansion, the dipole matrix element between two states is given by

$$\mu_{n'n,\mathbf{k}} = \mathcal{A} \int_{\mathcal{L}} dz \sum_{i,j} u_{i0}^* F_{m,i\mathbf{k}}^* \mathbf{d} u_{j0} F_{n,j\mathbf{k}}. \quad (3.79)$$

The question to answer is to whether the dipole operator is acting on the lattice periodic part u_{j0} or on the envelope part F_i . The issue has been addressed by Burt and others 11, 13, concluding that the expression is dominated by

$$\mu_{n'n,\mathbf{k}} \approx \frac{\mathcal{A}}{V_c} \sum_{i,j} \langle u_{i0} | u_{j0} \rangle_{V_c} \int_{\mathcal{L}} dz F_{m,i\mathbf{k}}^* \mathbf{d} F_{n,j\mathbf{k}}. \quad (3.80)$$

But, within a $\mathbf{k} \cdot \mathbf{p}$ calculation involving only single-band models for both, conduction and valence band, the last expression evaluates due to the orthog-

3.4. ~~CHAPTER 3~~ ELEMENTARY CARRIERS OPTICAL TRANSITIONS

onality of u_{c0} and u_{v0} to zero¹. Therefore, no transition between conduction- and valence subbands in such models would exist. The reason lies in the single-band approximation. While the wavefunction of e.g. conduction subbands is dominated by the envelope modulating u_{c0} , the interband dipole moment is dominated by the admixture of u_{v0} into the conduction subbands and u_{c0} into the valence subbands. Working within the 8×8 model would therefore resolve the problem.

A simpler solution, allowing to use non- 8×8 models without the pathological feature of vanishing transition probabilities, is to use the momentum- instead of the dipole matrix element. The relation can be derived using the Heisenberg equation of motion for the position operator r , given by

$$\frac{\partial}{\partial t} \mathbf{r} = \frac{i}{\hbar} [H, \mathbf{r}]. \quad (3.81)$$

Assuming that n and m are eigenfunctions of the Hamiltonian H with corresponding eigenenergies E_n and E_m , replacing the derivative of the position operator by the momentum operator and $H |m\rangle$ by $E_m |m\rangle$, one obtains

$$\langle n | \mathbf{p} | m \rangle = \frac{im}{\hbar} (E_n - E_m) \langle n | \mathbf{r} | m \rangle. \quad (3.82)$$

The electron dipole operator (electrons are negatively charged) is related to the position operator by $\mathbf{d} = e\mathbf{r}$ leading to

$$\langle n | \mathbf{d} | m \rangle = e \frac{\hbar}{im} \frac{\langle n | \mathbf{p} | m \rangle}{(E_n - E_m)}. \quad (3.83)$$

Within direct transitions, the energy difference $E_n - E_m$ can be replaced by the photon energy $\hbar\omega$, leading to the simple expression for $\boldsymbol{\mu}_{mn,\mathbf{k}}$ in terms of the momentum matrix element

$$\boldsymbol{\mu}_{mn,\mathbf{k}} = \frac{e}{im\omega} \mathbf{p}_{mn,\mathbf{k}}. \quad (3.84)$$

In the approximation of slowly varying envelopes, the derivatives of the en-

¹This fact also applies to 4×4 and 6×6 $\mathbf{k} \cdot \mathbf{p}$ valence band models.

3.4. DIPOLE MATRIX ELEMENT CARRIERS OPTICAL TRANSITIONS

velopes are small and the momentum matrix element is dominated by

$$\mathbf{p}_{mn,\mathbf{k}} \approx \frac{A}{V_c} \sum_{i,j} \langle u_{i0} | \mathbf{p} | u_{j0} \rangle_{V_c} \int_{\mathcal{L}} dz F_{m,i\mathbf{k}}^* F_{n,j\mathbf{k}}. \quad (3.85)$$

The momentum matrix elements are related via 3.25 to band structure parameters P , defined e.g. in 2.32. This approximation is commonly applied and is also used in the remainder of the thesis.

Beside the neglected derivatives of the envelopes, the approximation 3.85 neglects the effect of remote bands. 3.85 considers only transitions between zone-center functions u_{i0} included explicitly in the Hamiltonian. In the $\mathbf{k} \cdot \mathbf{p}$ envelope equations, the effect of remote bands is included using Löwdins perturbation theory. Therefore, beside the mixing of the explicitly considered states in the Hamiltonian, the zone-center functions away from k include remote contributions. Consequently, transitions between remote contributions have to be included in a consistent definition of the momentum matrix elements 19.

Put here the momentum matrix calculation in the 2 band model.

Chapter 4

Coulomb Correlated Optical Transitions

The preceding chapter only considered free carriers and omitted their Coulomb interaction. The Coulomb interaction leads to the formation of electron-hole pairs, also denoted as *excitons*. Due to their bound nature, the transition energy is lowered, leading to absorption below the fundamental band gap, while the correlated movement of the electron-hole pair increases the transition probability and consequently the transitions strengths. As in the previous chapter, the theory review is based mainly on (author?) [15, 27, 14, 26?].

The present chapter therefore focuses on the inclusion of such many body effects in the evaluation of optical properties. A large part of the theory presented in the preceding chapter can be recycled. In general, only the omitted two-particle interaction Hamiltonian H_2 in 3.9 needs to be added to the equation of motion for the microscopic polarization 3.64. The chapter is therefore structured as follows: first, the Coulomb Hamiltonian is derived for Bloch functions and transformed into the electron-hole picture. Then the Coulomb Hamiltonian is included into the equation of motion, and the so called Hartree-Fock approximation is performed along with the introduction of screening.

4.1 Second Quantization

4.1.1 Introduction

If n_i, \mathbf{k}_i denote the quantum number of a Bloch state, then the Coulomb Hamiltonian 3.9 can be written as

$$\hat{H}_2 = \frac{1}{2} \sum_{n_1 \mathbf{k}_1, n_2 \mathbf{k}_2, n_3 \mathbf{k}_3, n_4 \mathbf{k}_4} \langle n_1 \mathbf{k}_1 n_2 \mathbf{k}_2 | v | n_3 \mathbf{k}_3 n_4 \mathbf{k}_4 \rangle \hat{a}_{n_1 \mathbf{k}_1}^\dagger \hat{a}_{n_2 \mathbf{k}_2}^\dagger \hat{a}_{n_3 \mathbf{k}_3} \hat{a}_{n_4 \mathbf{k}_4} \quad (4.1)$$

and the matrix element of the Coulomb operator reads

$$\begin{aligned} \langle n_1 \mathbf{k}_1 n_2 \mathbf{k}_2 | v | n_3 \mathbf{k}_3 n_4 \mathbf{k}_4 \rangle &= \frac{e^2}{4\pi\epsilon_0} \int_{\Omega} \int_{\Omega} d\mathbf{r} dz d\mathbf{r}' dz' \varphi_{n_1 \mathbf{k}_1}^*(\mathbf{r}, z) \varphi_{n_2 \mathbf{k}_2}^*(\mathbf{r}', z') \\ &\cdot \frac{1}{|(\mathbf{r}, z) - (\mathbf{r}', z')|} \varphi_{n_4 \mathbf{k}_4}(\mathbf{r}, z) \varphi_{n_3 \mathbf{k}_3}(\mathbf{r}', z'). \end{aligned} \quad (4.2)$$

The Coulomb-potential is mainly long-range and therefore more or less constant within a lattice cell. Consequently, the lattice periodic part can be averaged over a single crystal cell. The integration is then performed over lattice averaged quantities, as suggested in 3.26. Therefore, rewriting 4.2 into a more suitable form including lattice cell averages, yields

$$\begin{aligned} \langle n_1 \mathbf{k}_1 n_2 \mathbf{k}_2 | v | n_3 \mathbf{k}_3 n_4 \mathbf{k}_4 \rangle &= \frac{e^2}{4\pi\epsilon_0} \int_{\Omega} \int_{\Omega} d\mathbf{r} dz d\mathbf{r}' dz' \frac{1}{\mathcal{A}^2} e^{i(\mathbf{k}_4 - \mathbf{k}_1) \cdot \mathbf{r}} e^{i(\mathbf{k}_3 - \mathbf{k}_2) \cdot \mathbf{r}'} \\ &\cdot g_{n_1 \mathbf{k}_1, n_4 \mathbf{k}_4}(z) g_{n_2 \mathbf{k}_2, n_3 \mathbf{k}_3}(z') \frac{1}{|(\mathbf{r}, z) - (\mathbf{r}', z')|} \end{aligned} \quad (4.3)$$

where $g_{n_1 \mathbf{k}_1, n_4 \mathbf{k}_4}(z) \approx \sum_i F_{n_1 \mathbf{k}_1, i}^*(z) F_{n_4 \mathbf{k}_4, i}(z)$ and $g_{n_2 \mathbf{k}_2, n_3 \mathbf{k}_3}(z')$ is defined accordingly. The next step is to get rid of the free directions \mathbf{r} and \mathbf{r}' , where the slowly varying part of the Bloch-function is given by the plane wave. The first step is to rewrite the term $\frac{1}{|(\mathbf{r}, z) - (\mathbf{r}', z')|}$ as $\frac{1}{\sqrt{(\mathbf{r} - \mathbf{r}')^2 + (z - z')^2}}$. Then, the integration over \mathbf{r}' is transformed into the integration over the distance between \mathbf{r} and \mathbf{r}' , $\mathbf{s} = \mathbf{r} - \mathbf{r}'$. So, instead of performing for every point \mathbf{r} the integration over \mathbf{r}' , one integrates for every point \mathbf{r} over all possible distances

s. This approach leads to several simplifications

$$\begin{aligned} \langle n_1 \mathbf{k}_1 n_2 \mathbf{k}_2 | v | n_3 \mathbf{k}_3 n_4 \mathbf{k}_4 \rangle &= \frac{e^2}{4\pi\epsilon_0} \int_{\mathcal{L}} \int_{\mathcal{L}} dz dz' \frac{1}{\mathcal{A}^2} g_{n_1 \mathbf{k}_1, n_4 \mathbf{k}_4}(z) g_{n_2 \mathbf{k}_2, n_3 \mathbf{k}_3}(z') \\ &\cdot \int_{\mathcal{A}} \int_{\mathcal{A}} d\mathbf{r} d\mathbf{s} \frac{1}{\sqrt{|\mathbf{s}|^2 + (z - z')^2}} e^{i(\mathbf{k}_4 + \mathbf{k}_3 - \mathbf{k}_1 - \mathbf{k}_2) \cdot \mathbf{r}} e^{i(\mathbf{k}_2 - \mathbf{k}_3) \cdot \mathbf{s}} \end{aligned} \quad (4.4)$$

The integration over \mathbf{r} and \mathbf{s} is decoupled and therefore the plane-wave leads to a delta function

$$\int_{\mathcal{A}} d\mathbf{r} e^{i(\mathbf{k}_4 + \mathbf{k}_3 - \mathbf{k}_1 - \mathbf{k}_2) \cdot \mathbf{r}} = \mathcal{A} \delta_{\mathbf{k}_4 + \mathbf{k}_3, \mathbf{k}_1 + \mathbf{k}_2}. \quad (4.5)$$

The remaining integration over z, z' and \mathbf{s} depends on the dimensionality of the system.

The Fourier transformation along the free direction \mathcal{A} defined in 3.20 is used to expand $\frac{1}{\mathbf{r}}$

$$\vartheta(\mathbf{s}, z, z') = \frac{1}{\sqrt{|\mathbf{s}|^2 + (z - z')^2}} = \sum_{\mathbf{q}} \vartheta_{\mathbf{q}}(z, z') e^{i\mathbf{q} \cdot \mathbf{s}} \quad (4.6)$$

in terms of its Fourier representation. Taking the integral over \mathbf{s}

$$\int_{\mathcal{A}} d\mathbf{s} \sum_{\mathbf{q}} \vartheta_{\mathbf{q}}(z, z') e^{i\mathbf{q} \cdot \mathbf{s}} e^{i(\mathbf{k}_2 - \mathbf{k}_3) \cdot \mathbf{s}} = \mathcal{A} \sum_{\mathbf{q}} \vartheta_{\mathbf{q}}(z, z') \delta_{\mathbf{k}_3 - \mathbf{k}_2, \mathbf{q}} \quad (4.7)$$

leads to another delta function, which can together with 4.5 be used to simplify 4.1 into

$$\hat{H}_2 = \frac{1}{2} \sum_{n_1, n_2, n_3, n_4} \sum_{\mathbf{k}, \mathbf{k}', \mathbf{q}} \Theta_{\mathbf{q}, \mathbf{k}, \mathbf{k}'}^{n_1, n_2, n_3, n_4} \hat{a}_{n_1 \mathbf{k} + \mathbf{q}}^\dagger \hat{a}_{n_2 \mathbf{k}' - \mathbf{q}}^\dagger \hat{a}_{n_3 \mathbf{k}'} \hat{a}_{n_4 \mathbf{k}}. \quad (4.8)$$

Here, \mathbf{k}_4 has been relabeled to \mathbf{k} and \mathbf{k}_3 to \mathbf{k}' . The term $\Theta_{\mathbf{q}, \mathbf{k}, \mathbf{k}'}^{n_1, n_2, n_3, n_4}$ contains all parts of 4.2 depending on actual wavefunctions and on the dimensionality of the nanostructure. It is given by

$$\Theta_{\mathbf{q}, \mathbf{k}, \mathbf{k}'}^{n_1, n_2, n_3, n_4} = \frac{e^2}{4\pi\epsilon_0} \int_{\mathcal{L}} \int_{\mathcal{L}} dz dz' g_{n_1 \mathbf{k} + \mathbf{q}, n_4 \mathbf{k}}(z) g_{n_2 \mathbf{k}' - \mathbf{q}, n_3 \mathbf{k}'}(z') \vartheta_{\mathbf{q}}(z, z'). \quad (4.9)$$

In the case of a bulk crystal, there is no integration over z, z' . Then, $\vartheta_{\mathbf{q}}^{3D}$ is given by the 3D Fourier transform of the Coulomb potential

$$\vartheta_{\mathbf{q}}^{3D} = \frac{4\pi}{\Omega q^2}. \quad (4.10)$$

The quantum well case has a 2D plane as the translational invariant directions and a 1D axis where symmetry is broken. The 2D Fourier transformation of 4.6 gives

$$\vartheta_{\mathbf{q}}^{2D}(z, z') = \frac{2\pi}{\mathcal{A}q} e^{-q|z-z'|}. \quad (4.11)$$

Hereby, the factor $\frac{2\pi}{\mathcal{A}q}$ denotes the Fourier transform of an ideal quantum well with no extension in the symmetry broken direction, while the exponential factor comprises of the finite extension of the quantum well wavefunctions.

Inspecting the Coulomb terms, it is clear that these terms diverge in the limit of $\mathbf{q} = 0$. The divergence can be resolved within the *Jellium model* (**author?**) [25], where the semiconductor is assumed to be intrinsically charge free. As a result, the diverging term of the electron-electron interaction at $\mathbf{q} = 0$ is canceled by the diverging term of the interaction of electrons with the homogeneous positive charge background. Hence, terms $\mathbf{q} = 0$ within the summation over \mathbf{q} are discarded.

4.1.2 Diagonal Approximation

The next approximation performed aims to remove two of the four subband indices in 4.8 by assuming that Coulomb interactions will not cause interband transitions. Then, $n_1 = n_4$ and $n_2 = n_3$, which is called here diagonal Coulomb approximation. This assumption is for example justified at an approximate level in symmetrical quantum wells, as the diagonal Coulomb matrix elements are due to the symmetry of the wavefunctions, two orders of magnitude larger than the off-diagonal (**author?**) [24]. Also, for single-band effective mass wavefunctions, only the diagonal terms remain, while others vanish due to the orthogonality of the zone-center functions. Using

this approximations, the Coulomb Hamiltonian reads

$$\hat{H}_2 = \frac{1}{2} \sum_{m,n} \sum_{\mathbf{k}, \mathbf{k}', \mathbf{q}} \Theta_{\mathbf{q}, \mathbf{k}, \mathbf{k}'}^{m,n,n,m} \hat{a}_{m\mathbf{k}+\mathbf{q}}^\dagger \hat{a}_{n\mathbf{k}'-\mathbf{q}}^\dagger \hat{a}_{n\mathbf{k}'} \hat{a}_{m\mathbf{k}}. \quad (4.12)$$

Consequently, the notation in mnmn $\Theta_{\mathbf{q}, \mathbf{k}, \mathbf{k}'}^{m,n,n,m}$ can be reduced to $\Theta_{\mathbf{q}, \mathbf{k}, \mathbf{k}'}^{m,n}$.

4.1.3 Holes

The next step is to transform the Coulomb Hamiltonian into the electron-hole picture. In the diagonal approximation 4.12, one distinguishes between electron states in the conduction bands c, d and hole states in the valence bands v, w . Therefore, the following four combinations are possible

$$n = c, m = d \quad n = c, m = v \quad n = v, m = c \quad n = v, m = w. \quad (4.13)$$

As next, hole operators are inserted for electrons in the valence band. Further, a natural ordering is reestablished by propagating the creation operators to the left and the annihilation operators to the right and setting the hole creation operator before, the hole annihilation operator after the one of the electron. The terms involving the sum $\sum_{n=c, m=d}$ are already in that ordering. Permuting the hole terms in the sum $\sum_{n=v, m=w}$ introduces a new two-operator term while the sums $\sum_{n=c, m=v}$ and $\sum_{n=v, m=c}$ can be summed together. Hence, the final Hamiltonian which will be used to calculate the

microscopic equation of motion is obtained as

$$\begin{aligned}
 \hat{H} = & \sum_{c,\mathbf{k}} E_c(\mathbf{k}) \hat{a}_{c\mathbf{k}}^\dagger \hat{a}_{c\mathbf{k}} - \sum_{v,\mathbf{k}} E_v(\mathbf{k}) \hat{b}_{v\mathbf{k}}^\dagger \hat{b}_{v\mathbf{k}} \\
 & - \mathbf{E}(\mathbf{r}, t) \cdot \sum_{c,v,\mathbf{k}} \boldsymbol{\mu}_{cv,\mathbf{k}} \hat{a}_{c\mathbf{k}}^\dagger \hat{b}_{v-\mathbf{k}}^\dagger + \boldsymbol{\mu}_{cv,\mathbf{k}}^* \hat{b}_{v-\mathbf{k}} \hat{a}_{c\mathbf{k}} \\
 & + \frac{1}{2} \sum_{c,d} \sum_{\mathbf{k}\mathbf{k}'\mathbf{q}} \Theta_{\mathbf{q},\mathbf{k},\mathbf{k}'}^{c,d} \hat{a}_{c\mathbf{k}+\mathbf{q}}^\dagger \hat{a}_{d\mathbf{k}'-\mathbf{q}}^\dagger \hat{a}_{d\mathbf{k}'} \hat{a}_{c\mathbf{k}} \\
 & + \frac{1}{2} \sum_{v,w} \sum_{\mathbf{k}\mathbf{k}'\mathbf{q}} \Theta_{-\mathbf{q},-\mathbf{k}'+\mathbf{q},-\mathbf{k}-\mathbf{q}}^{w,v} \hat{b}_{v\mathbf{k}+\mathbf{q}}^\dagger \hat{b}_{v\mathbf{k}'-\mathbf{q}}^\dagger \hat{b}_{w\mathbf{k}'} \hat{b}_{v\mathbf{k}} \\
 & \sum_{v,\mathbf{k}',\mathbf{q}} \Theta_{-\mathbf{q},-\mathbf{k}'+\mathbf{q},-\mathbf{k}}^{v,v} \hat{b}_{v\mathbf{k}'}^\dagger \hat{b}_{v\mathbf{k}'} \\
 & - \frac{1}{2} \sum_{\mathbf{k}\mathbf{k}'\mathbf{q}} \left\{ (\Theta_{-\mathbf{q},-\mathbf{k}'+\mathbf{q},\mathbf{k}}^{v,c} + \Theta_{\mathbf{q},\mathbf{k},\mathbf{q}-\mathbf{k}'}^{c,v}) \hat{a}_{c\mathbf{k}+\mathbf{q}}^\dagger \hat{b}_{v\mathbf{k}'-\mathbf{q}}^\dagger \hat{b}_{v\mathbf{k}'} \hat{a}_{c\mathbf{k}} \right\}.
 \end{aligned} \tag{4.14}$$

The indices \mathbf{k} and \mathbf{k}' have in some cases been swapped, shifted by \mathbf{q} and occasionally changed sign.

4.2 Transitions Calculation

4.2.1 Equations of Motion

The next task is to evaluate the equation of motion 3.57 for $\hat{p}_{nm,\mathbf{k}}$, as it has already been done in previous chapter, excluding the Coulomb interaction. Therefore, the remaining task is to evaluate the commutator of the microscopic polarization and the Coulomb Hamiltonian,

$$\frac{d}{dt} \hat{p}_{nm,\mathbf{k}} = \frac{i}{\hbar} \left[\hat{H}_2 \hat{p}_{nm,\mathbf{k}} \right] + rest \tag{4.15}$$

where \hat{H}_2 are the Coulomb terms in 4.14. The evaluation is straight forward but lengthy: For each four-operator term, one writes $\hat{H}_2 \hat{p}_{nm,\mathbf{k}} - \hat{p}_{nm,\mathbf{k}} \hat{H}_2$ and then permutes $\hat{p}_{nm,\mathbf{k}}$ in the first term to the left to obtain the remaining terms which do not cancel finally. The remaining terms are resorted at the end into the natural ordering. The resulting equation of motion is given by equation

number . Taking the two-band approximation of this particular equation and ignoring the k dependence of the Coulomb matrix element results in eq. (3.9) of [69]. Comparing this equation with the free-carrier result (4.74) reveals that in (5.21a), the valence band energy is shifted to

Chapter 5

Semiconductor Microcavity

Put intro here...

5.1 Optical Resonator

An optical resonator is a device used for confining light at certain frequencies. The classical resonator (such as the Fabry-Perot etalon seen in Fig. 5.1) consists of two planar mirrors, separated by a distance l . The region between the two mirrors is called the spacer layer and its refractive index is denoted by n . For now we assume that the medium outside the structure is plain air. The transmission spectrum of this structure exhibits a pattern of repetitive peaks of large transmission corresponding to resonances of the etalon. This varying transmission function is caused by an interference between the multiple reflections of light between the two reflecting surfaces (see Fig. 5.1). Constructive interference occurs if the transmitted beams are in phase, which corresponds to a high-transmission peak. For transmitted beams that are out-of-phase a destructive interference occurs, which corresponds to a minimum in the transmission spectrum. The multiple-reflected beams' phase matching depends on the wavelength λ of the light, the beam incidence angle θ , the etalon thickness l and the refractive index of the spacer material n .

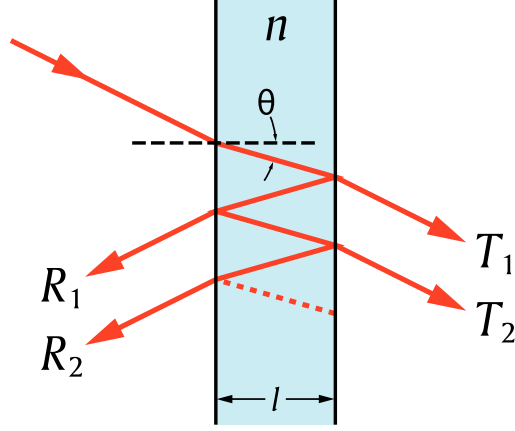


Figure 5.1: Fabri-Perot etalon multiple reflections.

The phase between each successive reflection is ?]

$$\delta = \left(\frac{2\pi}{\lambda} \right) 2nl \cos(\theta) \quad (5.1)$$

If both surfaces have reflectance R , the transmittance function of the entire structure is given by

$$T = \frac{(1 - R)^2}{1 + R^2 - 2R \cos(\delta)} = \frac{1}{1 + F \sin^2\left(\frac{\delta}{2}\right)}, \quad (5.2)$$

where $F = \frac{4R}{(1-R)^2}$ is the finesse coefficient. Fig. 5.2 shows the dependence of the transmittance on the phase parameter δ , for various values of R (or equivalently of F). The maximum transmission occurs when the optical path length difference $2nl \cos(\theta)$ between each transmitted beam is an integer multiple of the wavelength. In the absence of absorption, the reflectance of the structure R is the complement of the transmittance, i.e. $R + T = 1$. The maximum reflectivity is given by

$$R_{max} = 1 - \frac{1}{1 + F}, \quad (5.3)$$

which occurs when the path-length difference is equal to half an odd multiple of the wavelength.

5.2. DISTRIBUTED BRAGG REFLECTOR SEMICONDUCTOR MICROCAVITY

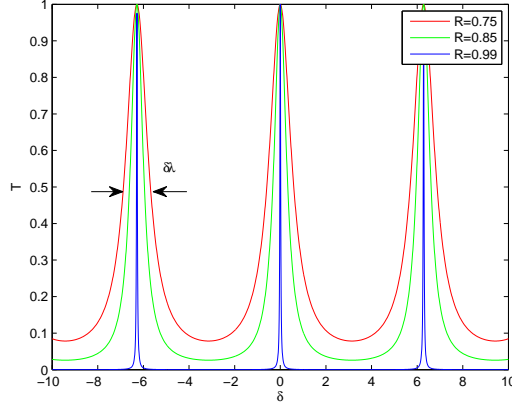


Figure 5.2: Resonator transmittance function for various values of mirror reflectance R . $\delta\lambda$ is the full-width half-maximum of the transmission band.

The wavelength separation between adjacent transmission peaks or free spectral range (FSR) of the etalon, $\Delta\lambda$, is given by

$$\Delta\lambda = \frac{\lambda_0^2}{2nl \cos(\theta) + \lambda_0}, \quad (5.4)$$

where λ_0 is the central wavelength of the nearest transmission peak. The FSR is related to the full-width half-maximum (FWHM) $\delta\lambda$ of any one transmission band by a quantity known as the *finesse*

$$\mathcal{F} = \frac{\Delta\lambda}{\delta\lambda} = \frac{\pi}{2 \arcsin(1/\sqrt{F})} \quad (5.5)$$

5.2 Distributed Bragg Reflector

The reflecting surfaces (or mirrors) modeled in previous section by a reflectivity parameter R are realized in practice by a stack of multiple layers of alternating semiconductor materials with varying refractive indices called Distributed Bragg Reflector (DBR) (see Fig. 5.3). The alternating high and low indices, denoted respectively by n_H and n_L , and the semiconductor layer

5.2. DISTRIBUTED BRAGG REFLECTOR MICROCAVITY

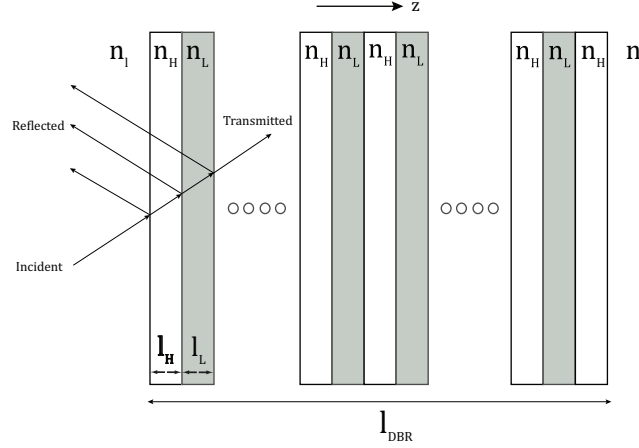


Figure 5.3: Schematic illustration of a Distributed Bragg Reflector (DBR). z represents the growth direction of the layered structure.

thicknesses satisfy the following condition

$$n_L l_L = n_H l_H = \frac{\lambda_c}{4}, \quad (5.6)$$

where λ_c is the center wavelength of the high reflectivity region of the structure. The two indices n_l and n_r are, respectively, the left- and right-hand cladding material refractive indices.

The principle of operation can be understood as follows. Each interface between the two materials contributes a Fresnel reflection. For the design wavelength λ_c , the optical path length difference between reflections from subsequent interfaces is half the wavelength; in addition, the reflection coefficients for the interfaces have alternating signs. Therefore, all reflected components from the interfaces interfere constructively, which results in a strong reflection. The reflectivity achieved is determined by the number of layer pairs and by the refractive index contrast between the layer materials. The reflection bandwidth is determined mainly by the index contrast, $n_H - n_L$.

In order to analyze the reflection and transmittance of the DBR, we use the Transfer Matrix formalism [?], as is described in the next section.

5.2.1 Transfer Matrix Method (TMM)

A monochromatic electric field of frequency ω propagating in a dielectric medium, assuming a frequency independent dielectric function, can be shown to satisfy the following wave equation

$$\nabla^2 \mathbf{E}(\mathbf{r}) + \frac{\omega^2}{c^2(r)} \mathbf{E}(\mathbf{r}) = 0, \quad (5.7)$$

where

$$\mathbf{E}(\mathbf{r}, t) = \Re \{ \mathbf{E}(\mathbf{r}) e^{i\omega t} \},$$

the speed of light in the dielectric $c(r) = c_0/n(r)$, c_0 being the speed of light in the vacuum and $n(r)$ the location dependent refractive index.

A medium consisting of pairs of two different dielectric materials with different refraction indices has a growth axis, \hat{z} , dependent refraction index, i.e. $n(r) = n(z)$. Therefore equation 5.7 can be written as

$$\nabla^2 \mathbf{E}(\rho, z) + \frac{\omega^2}{c^2(z)} \mathbf{E}(\rho, z) = 0. \quad (5.8)$$

Because of the translational invariance along the in-plane, the solution of Eq. 5.8 consists of plane waves along the in-plane direction. For a given in-plane wave vector $k_{||}$ (parallel to the dielectric layer plane) we can make the following ansatz for the solution

$$\mathbf{E}_{\mathbf{k}_{||}} = E_{\mathbf{k}_{||}, \omega}(z) e^{i\mathbf{k}_{||} \cdot \rho}. \quad (5.9)$$

Substituting into Eq. 5.8 yields the following one-dimensional equation

$$\frac{d^2 E_{\mathbf{k}_{||}, \omega}(z)}{dz^2} + \left(\frac{\omega^2}{c^2(z)} - k_{||}^2 \right) E_{\mathbf{k}_{||}, \omega}(z) = 0. \quad (5.10)$$

This equation can be solved separately for each layer of the stack. The solution for a homogeneous layer with a constant refractive index is of the

5.2. DISTRIBUTED-BRAGGER REFLECTOR INDUCTOR MICROCAVITY

form

$$\begin{aligned} E_{\mathbf{k}_{\parallel},\omega}(z) &= E^+ e^{ik_z z} + E^- e^{-ik_z z}, \\ k_z &= \sqrt{\frac{\omega^2}{c^2} - \mathbf{k}_{\parallel}^2}. \end{aligned} \quad (5.11)$$

The solution is a linear combination of two traveling waves in opposite direction along the \hat{z} axis. A non-evanescent wave solution exist only if $\frac{\omega}{c} > \mathbf{k}_{\parallel}$. The complex amplitudes of the forward (E^+) and backward (E^-) propagating waves are determined from the boundary conditions at each interface between two adjacent layers of the stack.

The relation between the two complex amplitudes between two point along the propagation direction, z_1 and z_2 , can be expressed as a 2×2 matrix transfer matrix. From here on we assume the non-unique basis for the transfer matrix is (E^+, E^-) . The transfer matrix takes into account the propagation through the dielectric media and the boundary conditions at each interface between two adjacent layers. The boundary conditions resulting from Maxwell's equations Put here the number of Maxwell's equations state that tangential components of the electric and magnetic fields are continuous across the interface. Further discuss the boundary conditions here The boundary conditions for the field components can be written as

$$\begin{aligned} D_{\perp 1} &= D_{\perp 2} \\ B_{\perp 1} &= B_{\perp 2} \\ E_{\parallel 1} &= E_{\parallel 2} \\ H_{\parallel 1} &= H_{\parallel 2} \end{aligned} \quad (5.12)$$

For simplicity we assume propagation only in the \hat{z} direction. The boundary conditions for the electric field become (see Fig. Schematic description of (a) light propagation through an interface between two adjacent dielectric

5.2. DISTRIBUTED BRAGG REFLECTOR CONDUCTOR MICROCAVITY

layers and (b) light propagation in a homogenous medium.

$$E_1^+ + E_1^- = E_2^+ + E_2^- \quad (5.13)$$

$$n_2 (E_2^+ - E_2^-) = n_1 (E_1^+ - E_1^-) \quad (5.14)$$

The interface transfer matrix M_i , for both linear polarizations of the field, TE and TM, can be written as

$$\begin{pmatrix} E_2^+ \\ E_2^- \end{pmatrix} = \frac{1}{2n_2} \begin{pmatrix} n_2 + n_1 & n_2 - n_1 \\ n_2 - n_1 & n_2 + n_1 \end{pmatrix} \begin{pmatrix} E_1^+ \\ E_1^- \end{pmatrix} \equiv M_i \begin{pmatrix} E_1^+ \\ E_1^- \end{pmatrix} \quad (5.15)$$

for a wave propagating from layer 1 to layer 2. The in-layer propagation transfer matrix M_p , which relates different vectors at z_1 and z_2 in the same layer can be written as (Fig. same figure as above, b)

$$\begin{pmatrix} E_2^+ \\ E_2^- \end{pmatrix} = \begin{pmatrix} e^{ikl} & 0 \\ 0 & e^{-ikl} \end{pmatrix} \begin{pmatrix} E_1^+ \\ E_1^- \end{pmatrix} \equiv M_p \begin{pmatrix} E_1^+ \\ E_1^- \end{pmatrix}, \quad (5.16)$$

where $k = (\omega/c_0) n$.

This amplitude propagation approach can be applied to the entire multilayer structure, for which the transfer matrix is simply the multiplication of M_i and M_p matrices for each boundary and layer

$$M_{DBR} = \prod_m M_{i,m} M_{p,m}, \quad (5.17)$$

where m is the dielectric layer index. The explicit relation between the amplitudes of the incident electric field in the DBR structure and the transmitted field on the other side can be written as

$$\begin{pmatrix} E_{out}^+ \\ 0 \end{pmatrix} = \begin{pmatrix} M_{11} & M_{12} \\ M_{21} & M_{22} \end{pmatrix} \begin{pmatrix} E_{in}^+ \\ E_{in}^- \end{pmatrix}. \quad (5.18)$$

The reflection and transmission coefficients of the entire structure can thus

5.2. DISTRIBUTED BRAGG REFLECTOR IN A SEMICONDUCTOR MICROCAVITY

be written as

$$r_{DBR} = -\frac{M_{21}}{M_{22}} \quad (5.19)$$

$$t_{DBR} = \frac{\det(M_{DBR})}{M_{22}} \quad (5.20)$$

The reflection coefficient can be expressed as $r_{DBR}(\lambda) = |r|e^{i\alpha_r}$. It can be shown that for a structure containing $2N + 1$ layers of high and low refractive indices (as in Fig. 5.3), so that the outermost layers are of high refractive index, n_H , and for the case of $k_i l_i = \frac{\pi}{2}$

$$|r| = \left(\frac{1 - \left(\frac{n_H}{n_L}\right)^{2N} \frac{n_H^2}{n_r n_l}}{1 + \left(\frac{n_H}{n_L}\right)^{2N} \frac{n_H^2}{n_r n_l}} \right)^2. \quad (5.21)$$

The phase within the region of high reflectivity (the *stop band*) of the reflector can be expressed as

$$\alpha_r = \frac{n_c L_{DBR}}{c} (\omega - \omega_c), \quad (5.22)$$

where L_{DBR} is the penetration depth into the DBR and is given by ?]

$$L_{DBR} = \frac{\lambda_c}{2} \frac{n_L n_H}{n_c (n_H - n_L)}. \quad (5.23)$$

As an illustration, we present in Fig. 5.4 an exact calculation of the reflection coefficient of a DBR containing 35 pairs of alternating high and low refractive index layers. The refractive indices for the simulation are $n_l = 1$ (air), $n_H = 3.45$ ($Al_{0.2}Ga_{0.8}As$), $n_L = 2.98$ ($AlAs$) and $n_r = 3.59$ ($GaAs$) (the structure refractive index profile is presented in (a)). In subplots (b) and (c) we plot the reflection coefficient as a function of the normalized wavelength, λ/λ_c , and the phase acquired by the electromagnetic field at each layer, $\phi = \frac{2\pi l_i n_i}{\lambda}$. The stop-band, as can be clearly seen from these plots, is centered at $\phi = \frac{\pi}{2}$, which corresponds to λ_c . In subplot (b) we also present the reflectivity phase α_r , where the zero-phase crossing is observed at λ_c as

5.2. DISTRIBUTED-BRAGG-REFLECTOR MICROCAVITY

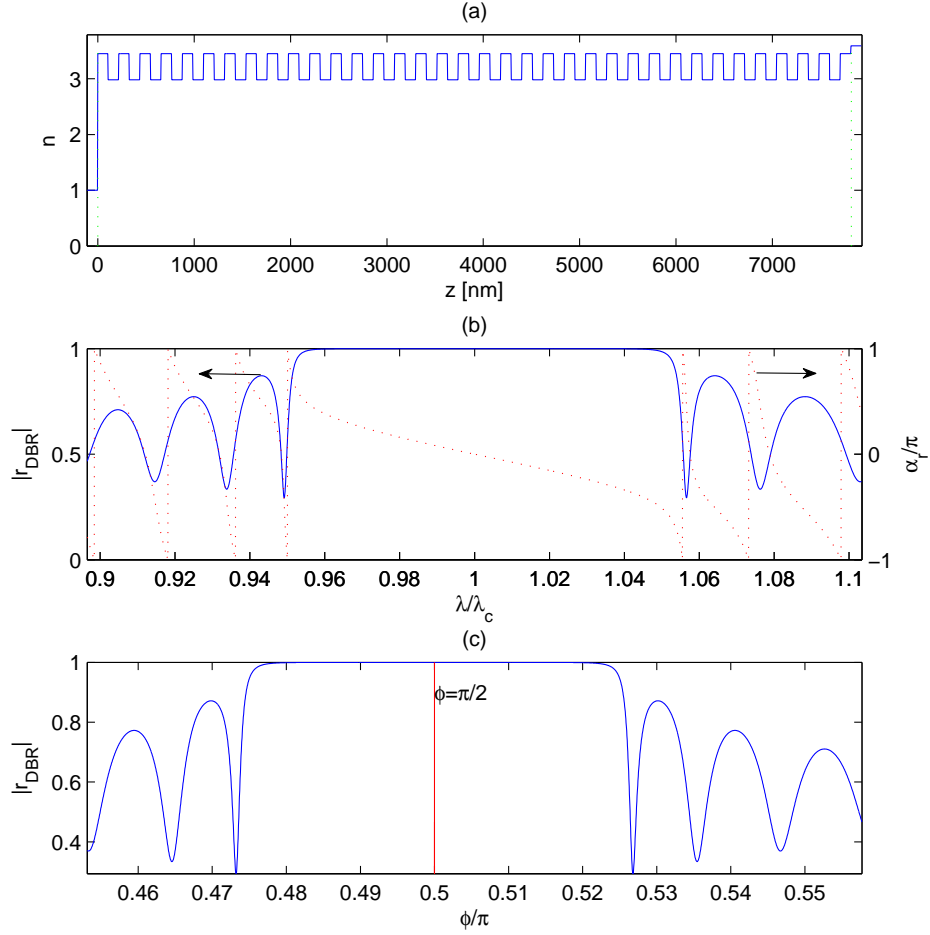


Figure 5.4: Simulation of a DBR structure with 35 alternating high and low layers, where (a) is the refractive index profile as a function of the growth axis, (b) the amplitude and phase of the normal incidence reflection function this structure as a function of normalized wavelength, λ/λ_c , and (c) the same amplitude as a function of the phase acquired by the EM field at each layer, $\phi = \frac{2\pi l_i n_i}{\lambda}$.

expected for the left-face reflection.

5.3 Microvity Optical Characteristics

5.3.1 Microcavity Reflection Spectrum

A microcavity (MC) is a Fabry-Perot resonator, whose mirrors are two DBRs and the spacer material is a semiconductor layer with refractive index n_c and of length $l_c = \frac{\lambda_c}{2n_c}m$ (m is a positive integer). The microcavity can be analyzed similarly to the DBR using the transfer matrix formalism. The MC's transfer matrix for a wave traveling from left to right can be written as

$$M_{MC} = M_{DBR}^r M_c M_{DBR}^l, \quad (5.24)$$

where M_c is the transfer matrix of the spacer (cavity) layer. We can write these three transfer matrices in their most general form as

$$M_{DBR}^r = \frac{n_c}{n_r} \begin{pmatrix} \frac{1}{t_r^*} & -\frac{r_r^*}{t_r^*} \\ -\frac{r_r}{t_r} & \frac{1}{t_r} \end{pmatrix}, \quad (5.25)$$

$$M_{DBR}^l = \frac{n_l}{n_c} \begin{pmatrix} \frac{1}{t_l^*} & \frac{r_l}{t_l} \\ \frac{r_l^*}{t_l^*} & \frac{1}{t_l} \end{pmatrix}, \quad (5.26)$$

$$M_c = \begin{pmatrix} e^{ikl_c} & 0 \\ 0 & e^{-ikl_c} \end{pmatrix}, \quad (5.27)$$

where (r_l, t_l) and (r_r, t_r) are, respectively, the reflection and transmission coefficients of the left- and right-hand DBR mirrors (see Fig. 5.5) and n_l and n_r are the left- and right-hand cladding material refractive indices, respectively.

Inserting these matrices into Eq. 5.24 yields

$$M_{MC} = \left(\frac{n_L}{n_H} \right)^2 \begin{pmatrix} \frac{e^{ikl_{eff}} - R^* e^{-ikl_{eff}}}{T^*} & \frac{r_l e^{ikl_{eff}} - r_r^* e^{-ikl_{eff}}}{t_l t_r^*} \\ \frac{r_l^* e^{-ikl_{eff}} - r_r e^{ikl_{eff}}}{t_l^* t_r} & \frac{e^{-ikl_{eff}} - R e^{ikl_{eff}}}{T} \end{pmatrix}, \quad (5.28)$$

where $T = t_l t_r$ and $R = r_l r_r$. l_{eff} is not equal to l_c but rather to $l_{eff} = l_c + l_p$,

5.3. MICROVITY OF A PERIODIC STRUCTURE FOR MICROCAVITY

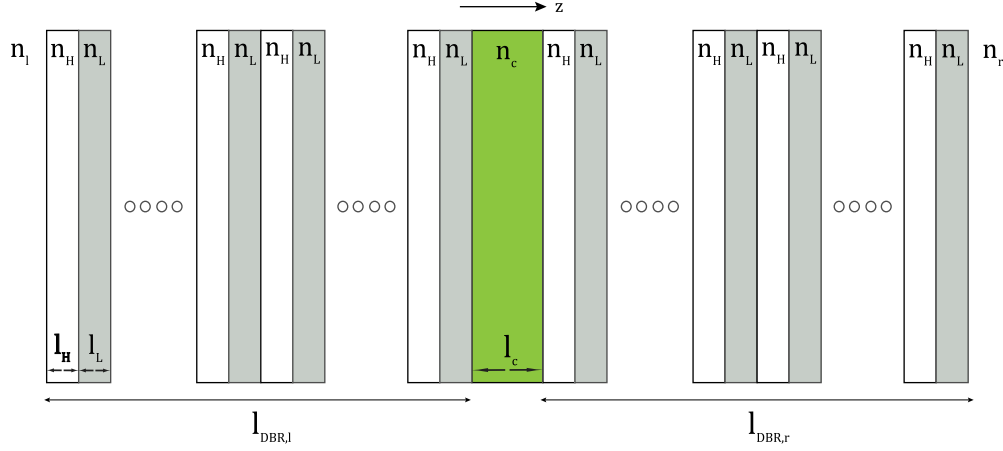


Figure 5.5: Microcavity schematic structure.

where l_p is the penetration depth of the cavity field into the DBR (**author?**) [40] and is given by

$$l_p = \frac{\lambda_c}{2} \frac{n_L n_H}{n_c (n_H - n_L)}. \quad (5.29)$$

The reflectance and transmittance of the MC can thus be written as

$$T_{MC} = \frac{1}{\det(M_{MC}) |M_{MC}^{22}|^2} = \frac{T}{(1 - R)^2 + 4R \sin^2(k_z l_{eff})} \quad (5.30)$$

$$R_{MC} = \frac{|M_{MC}^{21}|^2}{|M_{MC}^{22}|^2} = \frac{(|r_r| - |r_l|)^2 + 4R \sin^2(k_z l_{eff})}{(1 - R)^2 + 4R \sin^2(k_z l_{eff})} \quad (5.31)$$

It is clear that there are several modes which satisfy the condition $k_z l_{eff} = m\pi$. As we increase the number of layers in the DBR mirrors the stop-band reflectivity approaches unity and the cavity field reflection line becomes narrower. Because of the finite transmission probability of the DBR, the MC mode has a FWHM which can be shown to be (**author?**) [40]

$$2\gamma_c = \frac{1 - R_{MC}}{\sqrt{R_{MC}}} \frac{c}{n_c l_{eff}}. \quad (5.32)$$

γ_c is a homogenous lifetime broadening of the confined cavity mode, caused by the decay through the mirrors.

As an illustration, we present in Fig. 5.6 the simulation results of a

5.3. MICROVITY OF A PERIODICALLY STRUCTURED MICROCAVITY

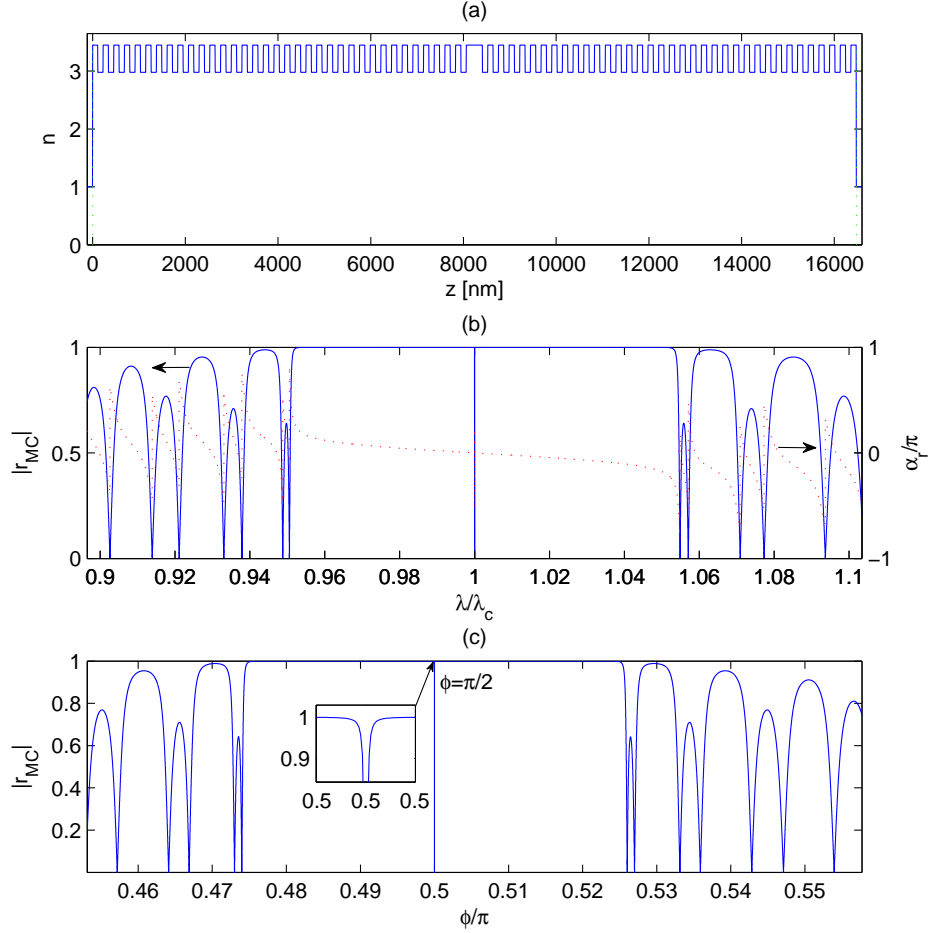


Figure 5.6: Simulation of a microcavity with two DBR's with 35 alternating high and low refractive index layers each, where (a) is the refractive index profile as a function of the growth axis, (b) the amplitude and phase of the normal incidence reflection function this structure as a function of normalized wavelength, λ/λ_c , and (c) the same amplitude as a function of the phase acquired by the EM field at each layer, $\phi = \frac{2\pi l_i n_i}{\lambda}$. The inset in (c) shows the reflection profile in the vicinity of $\phi = \frac{\pi}{2}$.

5.3. MICROVITY OF A PERPENDICULAR INDUCTOR MICROCAVITY

sample microcavity with two DBR mirrors with 35 alternating layers of high and low refractive index each and cavity length of $l_c = \frac{\lambda_c}{2n_c}$. This calculation was performed using the direct TMM calculation of the entire the structure, similarly to the DBR simulation presented above. The DBR parameters are the same as in Fig. 5.4, while for the cavity we choose $n_c = n_H = 3.45$ ($Al_{0.2}Ga_{0.8}As$).

5.3.2 Microcavity Confined Photon

The photon confinement along the \hat{z} axis leads to the following photon energy dispersion is (author?) [41]

$$E_{ph}(k_{\parallel}) = \frac{\hbar ck}{n_c} = \frac{\hbar c}{n_c} \sqrt{\left(\frac{2\pi m}{l_c}\right)^2 + k_{\parallel}^2}, \quad (5.33)$$

where m is a positive integer. For small k_{\parallel} we approximate the dispersion relation to a parabola

$$E_{ph}(k_{\parallel}) \cong \frac{2\pi\hbar c}{n_c l_c} \left(1 + \frac{\hbar^2 k_{\parallel}^2}{2m_{ph}}\right). \quad (5.34)$$

Here we define the photon in-plane effective mass $m_{ph} = \frac{\hbar n_c}{cl_c} \approx 10^{-5}m_0$, where m_0 is the free electron mass.

Bibliography

- [1] M. Altarelli. Electronic structure and semiconductor-semimetal transition in InAs-GaSb superlattices. *Physical Review B*, 28(2):842, July 1983. Copyright (C) 2010 The American Physical Society; Please report any problems to prola@aps.org.
- [2] Lucio Claudio Andreani, Alfredo Pasquarello, and Franco Bassani. Hole subbands in strained GaAs-Ga_{1-x}Al_xAs quantum wells: Exact solution of the effective-mass equation. *Physical Review B*, 36(11):5887, October 1987. Copyright (C) 2010 The American Physical Society; Please report any problems to prola@aps.org.
- [3] G. Bastard. Superlattice band structure in the envelope-function approximation. *Physical Review B*, 24(10):5693, November 1981. Copyright (C) 2010 The American Physical Society; Please report any problems to prola@aps.org.
- [4] G. Bastard. Theoretical investigations of superlattice band structure in the envelope-function approximation. *Physical Review B*, 25(12):7584, June 1982. Copyright (C) 2010 The American Physical Society; Please report any problems to prola@aps.org.
- [5] D. J. BenDaniel and C. B. Duke. Space-Charge effects on electron tunneling. *Physical Review*, 152(2):683, December 1966. Copyright (C) 2010 The American Physical Society; Please report any problems to prola@aps.org.
- [6] Gennadi Levikovich Bir, Grigori Ezekievich Pikus, Pesach Shelnitz,

- and David Louvish. *Symmetry and strain-induced effects in semiconductors*. Israel Program for Scientific Translations, 1976.
- [7] D. A. Broido and L. J. Sham. Effective masses of holes at GaAs-AlGaAs heterojunctions. *Physical Review B*, 31(2):888, 1985. Copyright (C) 2010 The American Physical Society; Please report any problems to prola@aps.org.
- [8] M. G. Burt. A new effective-mass equation for microstructures. *Semiconductor Science and Technology*, 3(12):1224–1226, 1988.
- [9] M. G. Burt. The justification for applying the effective-mass approximation to microstructures. *Journal of Physics: Condensed Matter*, 4(32):6651–6690, 1992.
- [10] M. G. Burt. Direct derivation of effective-mass equations for microstructures with atomically abrupt boundaries. *Physical Review B*, 50(11):7518, 1994. Copyright (C) 2010 The American Physical Society; Please report any problems to prola@aps.org.
- [11] M. G. Burt. Breakdown of the atomic dipole approximation for the quantum well interband dipole matrix element. *Semiconductor Science and Technology*, 10(4):412, 1995.
- [12] M. G. Burt. Fundamentals of envelope function theory for electronic states and photonic modes in nanostructures. *Journal of Physics: Condensed Matter*, 11(9):R53–R83, 1999.
- [13] M.G. Burt. The evaluation of the matrix element for interband optical transitions in quantum wells using envelope functions. *Journal of Physics: Condensed Matter*, 5(24):4091, 1993.
- [14] W. W. Chow and S.W. Koch. *Semiconductor-Laser Fundamentals*. Springer, 1999.
- [15] Shun Lien Chuang. *Physics of Optoelectronic Devices*. Wiley-Interscience, September 1995.

-
- [16] S.L. Chuang. Efficient band-structure calculations of strained quantum wells. *Physical Review B*, 43:9649–9661, 1991.
- [17] G. Dresselhaus. Spin-Orbit coupling effects in zinc blende structures. *Physical Review*, 100(2):580, October 1955. Copyright (C) 2010 The American Physical Society; Please report any problems to prola@aps.org.
- [18] P. Enders, A. Borwolff, M. Woerner, and D. Suisky. $\mathbf{k}\cdot\mathbf{p}$ theory of energy bands, wave functions, and optical selection rules in strained tetrahedral semiconductors. *Physical Review B*, 51(23):16695, June 1995. Copyright (C) 2010 The American Physical Society; Please report any problems to prola@aps.org.
- [19] P. Enders, A. B  rwolff, M. Woerner, and D. Suisky. $\mathbf{k}\cdot\mathbf{p}$ theory of energy bands, wave functions, and optical selection rules in strained tetrahedral semiconductors. *Physical Review B*, 51(23):16695, June 1995. Copyright (C) 2010 The American Physical Society; Please report any problems to prola@aps.org.
- [20] R. Eppenga. New $\mathbf{k}\cdot\mathbf{p}$ theory for GaAs/Ga_{1-x}Al_xAs-type quantum wells. *Physical Review B*, 36:1554–1564, 1987.
- [21] Bradley A. Foreman. Effective-mass hamiltonian and boundary conditions for the valence bands of semiconductor microstructures. *Physical Review B*, 48(7):4964, 1993. Copyright (C) 2010 The American Physical Society; Please report any problems to prola@aps.org.
- [22] Bradley A. Foreman. Exact effective-mass theory for heterostructures. *Physical Review B*, 52(16):12241, October 1995. Copyright (C) 2010 The American Physical Society; Please report any problems to prola@aps.org.
- [23] Bradley A. Foreman. Analytical Envelope-Function theory of interface band mixing. *Physical Review Letters*, 81(2):425, July 1998. Copyright (C) 2010 The American Physical Society; Please report any problems to prola@aps.org.

-
- [24] J. Hader, J. V. Moloney, and S. W. Koch. Microscopic theory of gain, absorption, and refractive index in semiconductor laser Materials-Influence of Conduction-Band nonparabolicity and Coulomb-Induced intersubband coupling. *IEEE Journal of Quantum Electronics*, 35:1878–1886, 1999.
- [25] Hartmut Haug and Stephan W Koch. *Quantum Theory of the Optical and Electronic Properties of Semiconductors*. World Scientific Publishing Company, 5 edition, April 2009.
- [26] S. W. Koch H. Haug. *Quantum Theory of the Optical and Electronic Properties of Semiconductors*. World Scientific Publishing Company, 5 edition, 2009.
- [27] J. D. Jackson. *Classical Electrodynamics*. John Wiley and Sons, Inc., 3rd edition, 1998.
- [28] E. O. Kane. *Handbook on semiconductors*, volume 1. W.Paul, 1982.
- [29] Evan O. Kane. Band structure of indium antimonide. *Journal of Physics and Chemistry of Solids*, 1(4):249–261, 1957.
- [30] M. Kira, F. Jahnke, W. Hoyer, and S. W. Koch. Quantum theory of spontaneous emission and coherent effects in semiconductor microstructures. *Progress in Quantum Electronics*, 23(6):189–279, November 1999.
- [31] O. Krebs and P. Voisin. Krebs and voisin reply:. *Physical Review Letters*, 82(6):1340, February 1999. Copyright (C) 2010 The American Physical Society; Please report any problems to prola@aps.org.
- [32] Per-Olov Lowdin. A note on the Quantum-Mechanical perturbation theory. *The Journal of Chemical Physics*, 19(11):1396–1401, November 1951.
- [33] J. M. Luttinger. Quantum theory of cyclotron resonance in semiconductors: General theory. *Physical Review*, 102(4):1030, May 1956. Copyright (C) 2010 The American Physical Society; Please report any problems to prola@aps.org.

-
- [34] J. M. Luttinger and W. Kohn. Motion of electrons and holes in perturbed periodic fields. *Physical Review*, 97(4):869, February 1955. Copyright (C) 2010 The American Physical Society; Please report any problems to prola@aps.org.
- [35] Paul C. Martin and Julian Schwinger. Theory of Many-Particle systems. i. *Physical Review*, 115(6):1342, 1959. Copyright (C) 2010 The American Physical Society; Please report any problems to prola@aps.org.
- [36] Richard A. Morrow and Kenneth R. Brownstein. Model effective-mass hamiltonians for abrupt heterojunctions and the associated wave-function-matching conditions. *Physical Review B*, 30(2):678, July 1984. Copyright (C) 2010 The American Physical Society; Please report any problems to prola@aps.org.
- [37] Joachim Piprek. *Semiconductor Optoelectronic Devices: Introduction to Physics and Simulation*. Academic Press, 2003.
- [38] G. B. Ren, Y. M. Liu, and P. Blood. Valence-band structure of wurtzite GaN including the spin-orbit interaction. *Applied Physics Letters*, 74(8):1117, 1999.
- [39] A. V. Rodina and A. Yu. Alekseev. Least-action principle for envelope functions in abrupt heterostructures. *Physical Review B*, 73(11):115312, March 2006. Copyright (C) 2010 The American Physical Society; Please report any problems to prola@aps.org.
- [40] V. Savona, A. Quattropani, and L. C. Andreani. Quantum well excitons in semiconductor microcavities: Unified treatment of weak and strong coupling regime. *Solid State Communications*, 93:733, 1995.
- [41] M. S. Skolnick, T. A. Fisher, and D. M. Whittaker. Strong coupling phenomena in quantum microcavity structures. *Semicond. Sci. Technol.*, 13:645–669, 1998.
- [42] Ratko G. Veprek, Sebastian Steiger, and Bernd Witzigmann. Ellipticity and the spurious solution problem of kbullp envelope equations. *Physical*

Review B, 76(16):165320, October 2007. Copyright (C) 2010 The American Physical Society; Please report any problems to prola@aps.org.

- [43] Peter Y. Yu, M. Cardona, and Manuel Cardona. *Fundamentals of Semiconductors: Physics and Materials Properties*. Springer-Verlag Telos, 2nd edition, May 1999.
- [44] Peter S. Zory, Paul F. Liao, and Paul Kelley. *Quantum Well Lasers*. Academic Press, April 1993.